



INTERNATIONAL ATOMIC ENERGY AGENCY
UNITED NATIONS EDUCATIONAL, SCIENTIFIC AND CULTURAL ORGANIZATION



INTERNATIONAL CENTRE FOR THEORETICAL PHYSICS
34100 TRIESTE (ITALY) - P.O.B. 588 - MIRAMARE - STRADA COSTIERA 11 - TELEPHONE: 2240-1
CABLE: CENTRATOM - TELEX 400892-1

H4.SMR/222 -6

SECOND AUTUMN WORKSHOP ON
CLOUD PHYSICS AND CLIMATE

(23 November - 18 December 1987)

GENERAL METEOROLOGY

J.B. OMOTOSHO
Dept. of Applied Geophysics & Meteorology
Federal University of Technology
Akure, Nigeria

1. ATMOSPHERIC DYNAMICAL, THERMODYNAMICAL AND PHYSICAL PROCESSES

Weather and Climate occur because air is constantly in motion. This motion occurs on a wide range of spectrum both in time and space, from the microscale up to the Rossby waves and the general circulation of the atmosphere. Our understanding of motions on each of these scales relies on the application of some of the physical concepts of hydrodynamics and thermodynamics.

The three basic principles governing the behaviour of the atmosphere are the conservation of (heat) energy, momentum and mass.

Energy conservation allows the study of the way and manner in which the net heat energy from the sun is utilised. In arriving at a balance, cognisance is taken of the roles played by the various gases which make up the atmosphere in effecting short-term physical and thermodynamical changes. By combining the mass and momentum equations with the energy equations, the way and direction of energy transformations in the atmosphere can be studied. This is the aim of this section.

1.1 The Basic Dynamical equations

The first conservation principle is that of momentum. For a non-inertial (relative) frame of reference, it is expressed as

$$\frac{d\mathbf{v}}{dt} = -\alpha \nabla p - 2\boldsymbol{\Omega} \wedge \mathbf{v} + \mathbf{g} \cdot \hat{\mathbf{k}} + \mathbf{F} \dots (1.1)$$

where \mathbf{v} - the velocity relative to the earth with components (u, v, w) .

\mathbf{g} - the gravitational acceleration

$\hat{\mathbf{k}}$ - a unit vector in the vertical

$\boldsymbol{\Omega}$ - the earth's angular velocity

\mathbf{F} - the frictional force on a unit mass of air

α - specific volume ($= 1/\rho$, ρ is density)

p - the pressure

Since large scale motions in the atmosphere are quasi-horizontal and follow essentially the earth's shape, (1.1) becomes, in component form in spherical co-ordinates (λ, ϕ, z) :

$$\frac{du}{dt} = -\alpha \frac{\partial p}{\partial x} - \frac{uw}{r} + \frac{uv}{r} \tan \phi - 2w \sin \phi \cos \phi + f_v + F_x$$

$$\frac{dv}{dt} = -\alpha \frac{\partial p}{\partial y} - \frac{vw}{r} - \frac{u^2}{r} \tan \phi - fu + F_y \dots (1.2a, b, c)$$

$$\frac{dw}{dt} = -\alpha \frac{\partial p}{\partial z} + \frac{u^2 + v^2}{r} - g + 2u \sin \phi \cos \phi + F_z$$

λ, ϕ represent longitude and latitude respectively.

Equations (1.2a, b, c) satisfy the angular momentum principle if we ignore the elliptic shape of the earth because the absolute velocity $(u + r \cos \phi)$ is not the true velocity to a non-rotating observer.

When terms of $\approx 10^{-3}$ are neglected (e.g. uw/r), the simplified equations are:

$$\frac{du}{dt} = -\alpha \frac{\partial p}{\partial x} + \left(f + \frac{u}{r} \tan \phi\right)v + F_x$$

$$\frac{dv}{dt} = -\alpha \frac{\partial p}{\partial y} - \left(f + \frac{u}{r} \tan \phi\right) u + F_y$$

$$0 = -\alpha \frac{\partial p}{\partial z} - g + F_z \quad \dots (1.3a, b, c)$$

Furthermore, for flows with Rossby number $R_o (= u/fL) \ll 1$, the geostrophic approximation may be obtained from (1.3a, b) as

$$\underline{V} = \frac{\alpha}{f} \hat{k} \wedge \nabla p \quad \dots (1.4)$$

and (1.3c) leads to the hydrostatic equation, on neglecting frictional effects:

$$g + \alpha \frac{\partial p}{\partial z} = 0 \quad \dots (1.5)$$

or, in pressure coordinates

$$\frac{\partial \phi}{\partial p} = -\alpha = -\frac{RT}{p} \quad \dots (1.6)$$

where R is the gas constant, T the temperature and ϕ , the geopotential, is given by:

$$\phi = \int_0^z g dz \quad \dots (1.7)$$

An alternative justification for (1.4) comes from consideration of the thermal stratification. When entropy S is used, the Brunt-Vaisala frequency N , may be expressed as:

$$N^2 = \frac{g}{c_p} \frac{\partial S}{\partial z} = \frac{g}{T} (\Gamma_d - \gamma)$$

where $\Gamma_d = g/c_p$ and $\gamma = -\frac{\partial T}{\partial z}$ are the dry adiabatic and environment lapse rates respectively. c_p is the specific heat at constant pressure. For typical γ of 6.5°C/Km , $N^2 \sim 10^{-8} \text{ s}^{-2}$. But $\Omega^2 \sim 10^{-9} - 10^{-9} \text{ s}^{-2}$. Hence $N^2 \gg \Omega^2$

In the tropical and equatorial regions however, (1.3a, b, c) are invalid since $f \sim 10^{-5}$ and hence $R_o \gg 1$. Moreover, dw/dt in

and very close to storms can be large ($\sim 0.1 \text{ ms}^{-2}$) while $w \sim 1-10 \text{ ms}^{-1}$. Thus equation (1.3) is totally unrealistic in the tropics and in such regions where the horizontal scale of the motion is less than about 300Km.

The second conservation principle concerns that of mass - the continuity equation. This may be expressed in the form

$$\frac{dp}{dt} + p \nabla \cdot \underline{V} = 0 \quad \dots (1.8)$$

When pressure is the vertical co-ordinate, equation (1.3a, b), with the quadratic and friction terms neglected, become in vectorial form

$$\frac{\partial \underline{V}}{\partial t} = -\nabla \phi - (\underline{V} \cdot \nabla) \underline{V} - \omega \frac{\partial \underline{V}}{\partial p} - f \hat{k} \wedge \underline{V} \quad (1.9)$$

and the conservation of mass then becomes

$$\nabla \cdot \underline{V} + \frac{\partial \omega}{\partial p} = 0 \quad \dots (10)$$

where $\omega = \frac{dp}{dt}$ and $\omega \approx -fgw$, since $\frac{\omega \partial p}{\partial x} \text{ etc} \ll w \frac{\partial p}{\partial z}$

A barotropic atmosphere is one in which there is no change of wind with height. From the thermal wind equation (obtainable from (1.4) and (1.6))

$$f \frac{\partial \underline{V}}{\partial \ln p} = -\hat{k} \wedge \nabla \frac{\partial \phi}{\partial p} \quad \dots (1.11)$$

we must have that

$$\hat{k} \wedge \nabla \frac{\partial \phi}{\partial p} \equiv \frac{R}{p} \hat{k} \wedge \nabla T = 0$$

hence $\nabla T \equiv 0$

The remaining conservation principle is represented by the First Law of thermodynamics. This will be expressed in terms of the potential temperature θ and entropy S as

$$\frac{ds}{dt} = c_p \frac{d}{dt} \ln \theta = \frac{Q}{T} \quad \dots (1.12)$$

$$\theta = T (1000/p)^k \quad \dots (1.13)$$

where $k = R/c_p$

Q is the diabatic heating rate. If (1.13) is differentiated as in (1.12) and combined with (1.6), we obtain

$$\begin{aligned} \frac{\partial}{\partial t} \left(\frac{\partial \Phi}{\partial p} \right) &= -\underline{V} \cdot \nabla \frac{\partial \Phi}{\partial p} - k \frac{Q}{p} \\ &\quad - \frac{\omega}{p} \frac{\partial}{\partial p} \left(p \frac{\partial \Phi}{\partial p} - k \Phi \right) \dots (1.14) \end{aligned}$$

Equations (1.6), (1.9), (1.10) and (1.14) provide a set of equations for the six unknowns u, v, w, p, ρ and T . They are the so-called primitive equations (Equation of state is implicit in (1.6)).

For mid-latitude synoptic-scale systems, the distribution of the geopotential Φ suffice to determine the fields of the geopotential tendency $(\partial \Phi / \partial t)$ and vertical motion ω . This is possible because the mid-latitude atmosphere is baroclinic and significant changes occur in z (or Φ) over short horizontal distances. The tropical atmosphere is, on the other hand,

quasi-barotropic. However, the temperature field shows weak (but sufficient) baroclinicity for the geostrophic approximation to be valid down to $10^\circ N$ (Omotosho, 1976). Nevertheless, existing height fields (or Φ) vary very little and equation (1.14) cannot be used as for the mid- and high latitudes. In tropical areas, the observed wind fields are more reliable than the geopotential heights (Burpee, 1972). This is so because the temperature error inherent in radio-sounde element makes it very difficult to analyse the geopotential field in low latitudes from the hydrostatic law. The magnitudes of such errors ($10^\circ C$ error leads to about 20 metres in Φ) are unacceptable as the amplitudes of synoptic scale weather systems in the tropics are rather small.

1.2 Vorticity Consideration

The relative vorticity ζ is highly correlated with synoptic-scale disturbances with large positive values associated with cyclonic storms (in the Northern Hemisphere). Since the absolute vorticity ζ_a is conserved following motion in mid-troposphere, the analysis and evolution of absolute vorticity forms the basis of dynamical forecast schemes. In the middle latitudes where the field of Φ suffice to determine $\frac{\partial \Phi}{\partial t}$ and ω , the quasi-geostrophic vorticity equation is very useful instead of the horizontal equations of motion. For a Beta-plane approximation, this is:

$$\frac{\partial}{\partial t} \nabla^2 \psi = -\underline{V}_\psi \cdot \nabla (\nabla^2 \psi + f) + f_0 \frac{\partial \omega}{\partial p} \dots (1.15)$$

where

$$\underline{V}_\psi = \underline{k}_\lambda \nabla \psi ; \nabla \cdot \underline{V}_\psi = 0 \dots (1.16)$$

and $\hat{k} \cdot \nabla_\perp \underline{v} = \nabla^2 \psi = \bar{\zeta}_g$

$$f_0 \nabla^2 \psi = \nabla^2 \Phi \quad \dots \dots (1.17)$$

ψ is the stream function and \underline{v} the non-divergent part of $\underline{v} (= \underline{v}_\psi + \underline{v}_\chi)$. f_0 is a constant value of the coriolis parameter - for motions with small latitudinal scale compared to the earth's radius.

$$(u_\psi = -\partial\psi/\partial y ; v_\psi = \partial\psi/\partial x)$$

For these systems, $\psi \approx \frac{R_0}{f_0}$ so that $\underline{v}_\psi \approx \frac{R_0}{f_0} \nabla \Phi / f_0$
Also in such motions, $|\nabla \cdot \underline{v}| \ll |\hat{k} \cdot \nabla_\perp \underline{v}|$ since the Rossby number R_0 is small.

In the case of the tropics, the vorticity equation which is found to be very useful and of better approximation to mid-tropospheric sy opticscale system outside convective or precipitating regions is the so-called Barotropic vorticity equation:

$$\frac{\partial}{\partial t} \nabla^2 \psi = - \underline{v}_\psi \cdot \nabla (\nabla^2 \psi + f) \quad \dots \dots (1.18)$$

This equation assumes that the flow is quasi-non divergent, but does not require quasi-geostrophy. In this case, the divergence and vorticity may be of same order of magnitude but the latter is usually larger than the divergence.

Writing (1.18) in the advective form, neglecting f and integrating over a closed domain σ gives

$$\int \frac{\partial \bar{\zeta}}{\partial t} d\sigma = - \int \nabla \cdot (\underline{v}_\psi \bar{\zeta}) d\sigma = - \int \bar{\zeta} (\underline{v}_\psi \cdot \hat{n}) dL \quad \dots (1.19)$$

where \hat{n} is a unit vector normal to the surface enclosed by L . Denoting the averaged value of $\bar{\zeta}$ over the domain by $\bar{\bar{\zeta}}$

where $\bar{\bar{\zeta}} = \int \bar{\zeta} d\sigma / \int d\sigma$

in (1.19) leads to a useful conservation property of the mean vorticity;

$$\frac{\partial \bar{\bar{\zeta}}}{\partial t} = 0 \quad \dots (1.20)$$

It may also be shown (using Gauss's-Div Theorem) after multiplying the simplified (1.18) by $\bar{\zeta}$ that

$$\frac{\partial}{\partial t} \left(\frac{\bar{\zeta}^2}{2} \right) = 0 \quad (\bar{\zeta}^2 \text{ is enstrophy}) \quad \dots (1.21)$$

and that, additionally, the mean kinetic energy $(\nabla \psi \cdot \nabla \psi / 2)$ of such flow is also conserved in the domain.

Thus when advection alone is considered in (1.18), no local time changes in the mean vorticity occurs.

The treatment presented here however allows no vertical coupling and is useful only for the level of non-divergence. However it is found to be a very good approximation of the motion in the tropics.

1.3 ENERGY CONSTRAINTS AND CYCLE

A very important link between the momentum conservation principle and the thermodynamic equation is the energy transformation process. This shows how thermal and kinetic energies are related through a conversion process, to satisfy the energy conservation principle. This is an important process for motions on all scales.

The Kinetic energy equation may be easily obtained from (1.19) and (1.10) as

$$\frac{\partial K}{\partial t} + \nabla \cdot \underline{V} K + \frac{\partial}{\partial p} \omega K = -\underline{V} \cdot \nabla \Phi + \underline{V} \cdot \underline{F} \quad \dots (1.22)$$

Multiplying (1.10) by Φ and adding to (1.22) leads, after some rearrangement, to a useful form of the energy equation:

$$\frac{\partial K}{\partial t} + \nabla \cdot [\underline{V}(K + \Phi)] + \frac{\partial}{\partial p} [\omega(K + \Phi)] = \omega \frac{\partial \Phi}{\partial p} + \underline{V} \cdot \underline{F} \quad \dots (1.23)$$

Again multiplying (1.10) by $C_p T$ and adding the result to the thermodynamic equation gives

$$\frac{\partial h}{\partial t} + \underline{V} \cdot \nabla (\underline{V} h) + \frac{\partial}{\partial p} \omega h = \omega \alpha + Q \quad \dots (1.24)$$

where $h = C_p T$ is the enthalpy, or simply potential energy.

Since $\alpha = \partial h / \partial p$ (equation (1.16)), comparison of (1.23) with (1.24) shows that Kinetic energy of motion is produced from potential energy through the term $\omega \alpha (= \omega RT/p)$. $\omega \alpha$ is commonly referred to as the energy conversion rate.

Integrating (1.23) over the entire atmosphere gives the rate of increase in mean Kinetic energy:

$$\frac{\partial}{\partial t} \int K dM = -R \int \frac{\omega T}{p} dM + \bar{F} \quad \dots (1.25)$$

(1.25) states that the direction of Kinetic energy change would depend on the correlation between ω and T . If warm air rises (as on the equatorward side of the Hadley cell) and cold air sinks, there will be an increase in mean Kinetic energy and this, by (1.24), will be at the expense of mean potential energy since $\overline{\omega \alpha} < 0$. Consequently, the Hadley circulation is called a thermally direct cell.

(1.25) also implies energy dissipation by friction forces.

Finally, adding (1.23) and (1.24) gives

$$\frac{\partial}{\partial t} (K + h) + \nabla \cdot [\underline{V}(K + \Phi + h)] + \frac{\partial}{\partial p} [\omega(K + \Phi + h)] = \bar{Q} + \underline{V} \cdot \underline{F} \quad \dots (1.26)$$

Integrating over entire atmosphere with $\omega = 0$ at $p = 0$ and $p = P_s$ (surface) and applying divergence theorem yields.

$$-\frac{1}{g} \frac{\partial}{\partial t} \iint (K + h) d\sigma dp = \bar{Q} + \bar{F} \quad \dots (1.27)$$

Thus the time rate of change of mean total energy is due only to diabatic heating and frictional forces. Hence for adiabatic and frictionless flow

$$\bar{K} + \bar{h} = \text{constant} \quad \dots (1.28)$$

and energy transformations is always between potential and kinetic energies.

Since only a very small fraction (1-2%) of atmospheric potential energy is actually available for conversion into Kinetic energy, the available potential energy, A (Lorenz, 1967) is introduced and may be expressed as

$$\frac{\partial A}{\partial t} = \frac{\partial}{\partial t} \left[\frac{C_p \overline{G} \overline{T'^2}}{2 \bar{T} (\bar{G} - \bar{P})} \right] \quad \dots (1.29)$$

is dry adiabatic lapse rate and T' is the departure of temperature from the mean. The energy equations may now be written simply as

$$\frac{\partial A}{\partial t} = g - c \quad \dots \quad (1.30)$$

$$\frac{\partial K}{\partial t} = c - d \quad \dots \quad (1.31)$$

$$\text{where } g = \left[\frac{Q^* \bar{T}''}{\bar{T}(\bar{T}_d - \bar{T})} \right]$$

is the generation (source) of A

c the conversion (sink) of A

d the dissipation of K.

A disadvantage of (1.29) occurs when $\bar{T}_d \rightarrow \bar{T}$, a situation frequently met in the low latitudes (Pearce, 1978). Application of the concept to convection in low latitudes is possible from Pearce's definition which partitions A into its baroclinicity (\bar{T}'^2) and static stability (\bar{T}''^2) components:

$$\frac{\partial A}{\partial t} = \frac{\partial}{\partial t} \left[\frac{C_T (\bar{T}'^2 + \bar{T}''^2)}{2 \bar{T}} \right] \quad \dots \quad (1.32)$$

where \bar{T} is a global average of T. \bar{T}' is associated with lapse rate changes only whereas \bar{T}'' is associated with horizontal temperature gradients.

Thus (1.30) and (1.31) each contain terms for zonal and eddy components of the flow. The directions of the complex energy exchanges in the atmosphere is shown in Figure 1.

1.4 RADIATIVE TRANSFER

All the motions, energy exchanges and transfers discussed above would not be possible but for the radiative absorption and transfer which take place between the earth and the atmosphere as a result of constant absorption of solar radiation and the emission of their own radiation to space.

The rate of energy transfer by electromagnetic radiation, the radiant flux F from the sun, is $3.90 \times 10^{26} \text{ W}$. This gives an irradiance E at the outer fringes of the sun ($r \sim 7 \times 10^8 \text{ m}$) of

$$E = F / 4\pi r^2 = 6.34 \times 10^7 \text{ W m}^{-2}$$

The irradiance E may be defined in terms of the monochromatic irradiance E_λ (irradiance per unit wavelength interval at wavelength λ) as

$$E = \int_0^\infty E_\lambda d\lambda \quad \dots \quad (1.33)$$

The radiance I, which is the irradiance per unit solid angle, is often very useful. E and I are related as

$$E = \int_0^{2\pi} I \cos \phi d\omega \quad \dots \quad (1.34)$$

$d\omega$ is the solid angle. $I \cos \phi$ is the component of the radiance normal to the surface at zenith angle ϕ .

A curve of E_λ vs λ is shown in Figure 2.

Figure 2 is also satisfied by Wien's displacement law that the wavelength of peak emission, λ_{\max} is higher at lower emission temperatures:

$$T \lambda_{\max} = \text{constant} \quad \dots \quad (1.35)$$

The dependence of (blackbody) emission upon temperature is obtained from Planck's Law for monochromatic irradiance at temperature T to give Stefan-Boltzmann law:

$$\pi E^* = \sigma T^4 \quad \dots (1.36)$$

where E^* is the integral of Planks equation over all wavelengths, that is,

$$E^* = \int_0^\infty E_\lambda^* = \int_0^\infty \frac{C_1}{\lambda^5 \exp(C_2/\lambda T)}$$

C_1 and C_2 have values $3.74 \times 10^{-16} \text{ Wm}^{-2}$ and $1.44 \times 10^{-2} \text{ m}^{\circ}\text{K}$ respectively.

The ratio of absorbed to incidence irradiance on a body is known as its absorptivity a_λ , while the strength, of the radiation emitted by the body depends on its emissivity E_λ .

If a body radiates as much heat energy as it absorbs, it is a blackbody. Kirchhoff's Law states that any body which absorbs strongly at a particular wavelength will also radiate strongly at that wavelength.

In this case

$$a_\lambda = E_\lambda \quad \dots (1.37)$$

Kirchhoff's Law is applicable to the atmosphere below 60km height.

For a non-opaque layer, the incident monochromatic irradiance at any wavelength may be absorbed, reflected or transmitted. Thus $E_\lambda(\text{absorbed}) + E_\lambda(\text{reflected}) + E_\lambda(\text{transmitted}) = E_\lambda(\text{incident})$. Since $E_\lambda(\text{absorbed})/E_\lambda(\text{incident}) = a_\lambda$ etc, we have that

$$a_\lambda + \epsilon_\lambda + \tau_\lambda = 1 \quad \dots (1.38)$$

τ_λ is the transmissivity of the layer. For an opaque surface $\tau_\lambda = 0$. In a plane parallel atmosphere uniform in the horizontal, absorption of radiation in the vertical is given by Beer's (or Lambert's) Law:

$$dE_\lambda = -E_\lambda k_\lambda \rho dz \quad \dots (1.39)$$

where k_λ is the absorption coefficient at wavelength λ and is related to the optical depth χ as

$$\chi_\lambda = \int_0^\infty \rho k_\lambda dz \quad \dots (1.40)$$

Integration of (1.39) yields

$$E_\lambda = E_{\lambda_0} \exp(-\chi_\lambda) \quad \dots (1.41)$$

Terrestrial Radiation

The foregoing treatment applies to solar radiation though the atmosphere for which atmospheric absorption is important but emission is negligible. Because of the diffuse nature of terrestrial radiation, both emission and absorption are important and calculations usually involve integration over a solid angle. The problem simplifies to a one-dimensional one if we consider the upward and downward fluxes (i.e. $\int I(\phi) \cos \phi d\omega$) at the downward and upward facing hemispheres. The assumption of course is one of a plane parallel atmosphere. The resulting equation of transfer is then the difference between the emission and the absorption:

$$dI_{\lambda} = -k_{\lambda}(\rho I_{\lambda} - \rho E^*) \quad \dots (1.42)$$

where the blackbody monochromatic emission E^* is given by (1.36). From (1.40), (1.42) may be expressed as

$$\frac{dI_{\lambda}}{d\gamma_{\lambda}} = I - E^* \quad \dots (1.43)$$

Equation (1.42) or (1.43) is known as the Schwarzschild's equation.

The radiative treatment presented above for both solar and terrestrial assumes a non-scattering atmosphere. This is of course unrealistic since significant scattering of radiation occurs in the atmosphere by air molecules and dust particles. Also, a constant absorption coefficient is assumed which again is not the case since absorber gas concentration varies in the vertical. Major absorbers are water vapour, clouds and ozone.

A more realistic approach is to be able to find the radiation intensity at any given level in the atmosphere with any composition and vertical structure. This is demonstrated in the lecture series on Satellite Meteorology.

When the necessary transfer calculations are made, it is then possible to deduce the contribution of radiative processes to the atmospheric energy budget and their role in the conservation laws discussed earlier in this section.

2. INSTABILITY MECHANISMS

Instability processes are very important in the atmosphere because they allow the origin of disturbances on various space and time scales to be determined from the flow thermodynamics and hydrodynamics. Ordinary diagnostic methods of the quasi-geostrophic theory only serve to account for the maintenance of, and relationships between, velocity, pressure and temperature fields.

2.1 Baroclinic Instability

The middle latitude atmosphere is baroclinic and (baroclinic) waves which amplify through the loss of potential energy of the basic flow develop within the zonal flow. Horizontal temperature advection plays a crucial role in the development of baroclinic waves. Baroclinic instability in zonal flows was studied independently at about same time by Charney (1947) and Eady (1949), the latter providing our present understanding of the origin of cyclone waves while Charney's work dealt with longer waves.

Eady's treatment may be summarised very simply by starting with the simplified vorticity, thermodynamic and continuity equations in x, y, z, t (in which set $Ro \ll 1$ and f is constant). There are

$$\frac{\partial \zeta}{\partial t} + \mathbf{V}_h \cdot \nabla \zeta - f \frac{\partial w}{\partial z} = 0 \quad \dots (2.1)$$

$$\frac{\partial S}{\partial t} + \mathbf{V}_h \cdot \nabla S + wB = 0 \quad \dots (2.2)$$

$$\frac{\partial u}{\partial x} + \frac{\partial v}{\partial y} = 0 \quad \dots (2.3)$$

The equation satisfied by the perturbation stream function ψ (assumed geostrophic) may be expressed by the single linear equation:

$$\left(\frac{\partial}{\partial t} + u \frac{\partial}{\partial x} \right) \left(\nabla^2 \psi + \frac{f^2}{gB} \frac{\partial^2 \psi}{\partial z^2} \right) = 0 \quad \dots (2.4)$$

where

$$\begin{aligned} B &= \frac{1}{\theta} \frac{\partial \theta}{\partial z} = \frac{\partial S}{\partial z} \\ \psi &= \frac{\theta}{f} \Delta S \\ \xi &= \nabla^2 \psi \end{aligned} \quad \dots (2.5)$$

and

$$\begin{aligned} \frac{\partial u}{\partial z} &= -\frac{g}{f} \frac{\partial}{\partial y} (\Delta S) \\ \frac{\partial v}{\partial z} &= \frac{g}{f} \frac{\partial}{\partial x} (\Delta S) \end{aligned}$$

(In terms of pressure, it can be shown that $\psi \propto \Delta p$).

With a solution of the form,

$$\psi = F(z) \exp(iy) \exp[ik(x-ct)] \quad \dots (2.6)$$

representing a wave moving in the x-direction with phase speed C_1 ($C = C_1 + C_2$), Eady showed that only waves with wavelengths λ satisfying

$$\lambda \geq \frac{\pi H}{f} \sqrt{gB} \quad \dots (2.7)$$

can amplify. H is the scale height ($\sim 10\text{Km}$). Thus λ increases with static stability. For typical values of B and f , the lower cut-off wavelength $\lambda_c = 4000\text{Km}$, with an e-folding time of about 2 days. In such waves, the trough axis tilts westwards with height.

The characteristics of the cyclones waves of the middle latitudes are very much similar to those of the theory, with much the same transfer properties.

Channey's theory provided the upper cut-off wavelength and thus completed the fundamental theory of baroclinic instability (See also Holton, J.R. (1972) for a 2-level quasi-geostrophic treatment).

In baroclinic instability, the waves amplify because the potential energy of the basic flow is converted into perturbation potential energy which is then converted into eddy kinetic energy, via equations (1.30) & (1.31).

2.2 Barotropic Instability

A barotropic atmosphere is one in which there is no vertical shear of the wind - ie the thermal wind is zero. Unlike the mid-latitudes where strong latitudinal temperature gradients provide the primary energy source for synoptic

scale disturbances, temperature gradients in tropical regions are small, leading to small available potential energy storage. Energy for disturbances thus comes primarily from latent heat release.

Since most tropical disturbances develop in situ, their development cannot usually be accounted for by baroclinic instability processes.

It is now established that barotropic instability and conditional instability of the Second Kind (CISK) are two main mechanisms for their initiation. The latter is treated in section 2.4

Starting from the barotropic vorticity equation (1.18) and introducing perturbation velocities as for the quasi-geostrophic theory (but here, no assumption of geostrophy) the linearised perturbation stream function equation may be expressed as

$$\left(\frac{\partial}{\partial t} + \bar{u} \frac{\partial}{\partial x} \right) \nabla^2 \psi + \left(\beta - \frac{d^2 \bar{u}}{dy^2} \right) \frac{\partial \psi}{\partial x} = 0 \quad (2.8)$$

Kuo (1949) showed that barotropic instability of the zonal flow is possible if

$$\beta - \frac{d^2 \bar{u}}{dy^2} = \frac{d}{dy} (\bar{\zeta} + f) = 0 \text{ somewhere} \quad (2.9)$$

That is, the profile of absolute vorticity must change sign somewhere within the domain of interest (a full treatment of this is in Holton, J.R. (1972) p. 290). Such profiles, take from Resnick (1976), are shown in Figure 3 which shows that the condition for instability is met only in the month of August at 700mb at longitude 5°E.

Resnick has shown, however, that tropical zonal flows do satisfy the conditions for both barotropic and baroclinic instabilities. That is, that even though horizontal temperature gradients may be small, they are nevertheless sufficient to give some vertical shear of the wind in addition to lateral wind shear. In fact, strong vertical shear exists over West Africa and Eastern Atlantic as evident on Figure 8b.

That this is so was shown by Charney (1973) using the internal jet theory of Charney and Stern (1962). The condition here is that the gradient of potential vorticity \bar{q} must be negative somewhere in the domain:

$$\frac{\partial \bar{q}}{\partial y} = \frac{\partial}{\partial y} (\bar{\zeta} + f) + \frac{\partial}{\partial p} \left(\frac{p f_0^2}{R \sigma} \frac{\partial \bar{u}}{\partial p} \right) \quad (2.10)$$

where f_0 is the Coriolis parameter at the centre of the region and σ is static stability defined by $\sigma = T \partial \bar{\theta} / \bar{\theta} \partial p$. The resulting field of $\partial \bar{q} / \partial y$ at 700mb is shown in Figure 4, giving firm indication that although both types of instability are important, the baroclinic term nevertheless makes a smaller contribution.

2.3 Convective Instability

Embedded within the synoptic scale systems are meso-scale convective circulations whose initiation and evolution are determined by the stability control of the larger-scale flow and the release of latent heat. In an unsaturated atmosphere, static instability occurs only when, for the lapse

rate γ given

$$\text{by } \gamma = \Gamma_d - \frac{1}{\theta} \frac{\partial \bar{\theta}}{\partial z}, \quad \dots \quad (2.11)$$

$$\frac{\partial \theta}{\partial z} < 0$$

However, continuous parcel ascent will lead to condensation and latent heat release. Instability continues in this saturated situation if the lapse rate is greater than the saturated adiabatic lapse rate Γ_s . The stability condition for such a moist atmosphere is then known as Conditional Instability (i.e. $\Gamma_d > \gamma > \Gamma_s$). This is more conveniently represented in terms of the equivalent potential temperature θ_e which is the temperature an air parcel would have if all its moisture were condensed out and then brought dry adiabatically down to 1000mb level. The process is irreversible. θ_e is given by

$$\theta_e = \theta \exp(Lq_s/c_p T)$$

and conditional instability occurs if

$$\partial \theta_e / \partial z < 0$$

It is stable (absolutely) otherwise. This is also known as convective instability. Figure 5 shows that the tropical atmosphere is conditionally unstable in the lower troposphere. However, the release of the instability additionally requires low-level convergence to ensure (forced) lifting to saturation. This is because only air below about 900mb has sufficiently high to become convectively buoyant when forced to rise; much more forced ascent is required for higher layers due to the low .

2.4 Convective Instability of the Second Kind (CISK)

In the previous two subsections, it was emphasised that, unlike for the mid-latitude synoptic scale systems, latent heat is the major energy source for many tropical circulations. The convective systems are embedded in and controlled by the larger-scale flow.

In this type of arrangement, strong interactions exist between the smaller and the larger circulations.

Charney and Eliassen (1964) had shown that ordinary conditional (or convective) instability produces significant growth rate only on the scale of individual cumulus clouds. This is especially so for reasons given in the previous section. The convergence required is on a larger scale and is frictionally driven. With considerable ascent thus ensured, attainment of buoyancy by the rising air parcel is possible and the condensing cloud air then supplies (latent) heat to the larger-scale flow. The interaction is thus co-operative; the larger scale motion supplies needed moisture for cumulus growth through frictional convergence and Ekman pumping while the cumulus clouds in turn supply the latent heat required to drive the large scale circulation.

When such co-operative interaction leads the unstable growth of the larger-scale system, the process is referred to as Conditional Instability of the Second Kind (CISK).

3. TROPICAL METEOROLOGY

The weather and climate of the tropics and subtropics are influenced mainly by the trades of both hemispheres - the north-east and south-east trades. The latent changes direction on crossing the equator to become southwesterly flow, popularly known as the southwest monsoon. The marked contrast between the air mass properties (direction and moisture) gives rise to a kind of pseudo-frontal zone - the Inter-Tropical Convergence Zone, ITCZ - where the two trades meet. In West Africa, the continental manifestation of the ITCZ is called the Inter-Tropical Discontinuity, ITD.

It is the seasonal and daily meridional oscillations of the ITCZ or ITD that essentially determine the weather and rainfall patterns of the semi-arid and disturbed areas of the tropics. The location of this zone is shown in Figure 6 for both summer and winter months. A mechanism of ITCZ formation and maintenance was put forward by Charney (1967). Since the low-level tropical air is highly moisture-laden and is convectively unstable (section 2.3), cumulus convection and latent heat release depend largely on frictional pumping of mass and moisture out of the layer. These are proportional to the vorticity of the surface wind and may be expressed simply as

$$\omega_0 = A \zeta_0 \quad \dots \quad (3.1)$$

where A depends on the Kinematic coefficient of eddy viscosity (K_M) and the cross-isobaric angle (α) of the winds. Thus in a tropical atmosphere with positive vorticity imparted by a disturbance, frictional convergence will lead to upward pumping

of moist air and cloud formation. The clouds in turn generate condensational warming, fall of pressure and further intensification of the cyclonic vorticity and hence convergence, leading to a perpetuation of the system. This is the CISK process discussed in section (2.4).

However, some of the characteristics of the ITCZ differ significantly from those of the ITD. While weather and precipitation occur in the immediate vicinity of the former, significant weather is not encountered for about 150km south of the surface ITD (Hamilton & Archbold, 1945; Adejokun, 1966). Associated with the surface convergences are low-pressure systems whose intensity usually increases with height before weakening. Also, much of the tropical rainfall is from convective clouds (see e.g. Glatz, 1976; and Omotosho, 1985 for the West African case) of varying dimensions and intensities and are known to be associated with the synoptic-scale pressure disturbances and the monsoons.

In order to get full appreciation of the development and evolution of each of the rain-producing systems and their relative contribution to the precipitation of the semi-arid regions, each system will be treated separately. This is because the semi-arid zones, especially the continental areas, receive meagre but very vital precipitation when the appropriate flow region around the ITCZ or ITD reaches and encompasses the zone. It is also important to note that the meridional oscillation of the ITCZ or ITD is itself dependent on the seasonal variations of the subtropical anticyclonic centres; the failure of these centres to shift appreciably northwards have often led to disastrous rainfall deficits in the semi-arid regions of West Africa.

Thus, we shall discuss the following groups of rain-producing tropical circulations:

- (a) the monsoons
- (b) synoptic-scale wave disturbances (easterly waves);
- (c) meso-scale convective weather systems (thunderstorms, squall lines and cloud clusters)
- (d) Tropical cyclones

3.1 THE MONSOONS

Similar to the day and night cycles of the sea breeze, we observe a summer and winter monsoon. The summer monsoon represents large scale cross-equatorial flow of air from the oceans to the tropical areas of the Middle East, particularly India, Southern Asia and also West Africa. It is a time of wide-spread and prolong precipitation because, as shown by Lettan (1956), large-scale flows with strong westerly components are usually associated with vertically increasing kinetic energy of the perturbation upward motion as:

$$\frac{\partial}{\partial z}(w'^2) = 2u\Omega \cos \phi$$

where w' is the perturbation vertical velocity, u is the zonal component of the wind and ϕ is the latitude.

The winter monsoon is a similar large scale flow but in the reverse direction from land to sea from a belt of high pressure which extends to cover the above regions. Unlike the summer monsoon, it is a period of complete dryness and frequent dust over West Africa but is a 'shirt' rain period else here affected by the monsoon. The monsoon regions of

world are shown in Figure 7. The ocean surface temperature, ITCZ positions, land/sea temperature contrasts and the interactions with the trade wind regime are some of the important processes which combine to determine the characteristics of the monsoon circulations.

(a) The Indian Monsoon

A primary factor which governs all synoptic weather systems of the monsoon period is the very strong and rather permanent easterly circulation at the upper troposphere during this season. The wind field is so strong that no synoptic systems are observed between 300 and 100 hpa. The monsoon depressions which travel from the Bay of Bengal through north-central India fall into this category. Their structure in many ways resemble that of the African easterly wave perturbation except that here the cyclonic vortex is deeper and the equatorial westerlies extend to about 500 hpa.

The major feature of the circulation over southern Asia is depicted in Figure 8. At the surface and low level, the monsoon is characterised by a semi-synoptic scale low pressure (Figure 9a) which is most intense in the 800 - 600 hpa layer (Ramage, 1971).

The onset of monsoon over India appears to be in a 'burst', often accompanied by violent squalls and occasional intense cyclones. Surface temperature falls with monsoon onset. The disturbance lasts for upto a week, causing widespread rainfall, at the peak of monsoon. Perhaps the most significant feature of the monsoon onset over Indian is the appearance of an

equatorial jet at 150hpa which is connected with the formation of an upper level high pressure system over the Tibetan Plateau during the summer months. In winter time, the westerly jet more or less cycles the southern rim of the Himalayas (Figure 9b) with the streamlines defining the mountain contour very well.

In summer however, a completely different picture emerges with the westerly jet now to the north of the mountains and the appearance of the aforementioned equatorial easterly jet at 150hpa level. The southwest monsoon circulation is thus reinforced. The strong low-level convergence combined with the active divergence in the upper-level easterlies leads to strong upward motion which is also intensified by the large latent heat release due to the large moisture convergence.

Recently, the vagaries of the monsoon have been linked with the Southern Oscillation Index and the El Nino events (WMO, 1987). It has been shown by Shukla and Paolino (1983) that weak monsoon years are associated with above-normal pressure and vice versa, and that most of the severe drought years over India were associated with El Nino events. In fact, only six of the El Nino years had above-normal rainfall.

The retreat of the monsoon from over northern India is indicated by the weakening and eventual disappearance of the easterly jet.

(b) The West African Monsoon

The West African monsoon occurs on a relatively smaller scale than its Asian component. The seasonal shift of the low pressure centre is only about 17° latitude compared to about

30° for that of the Indian monsoon. The depression here is essentially a heat low, as the zones of maximum temperature in both winter and summer are almost coincident with the low pressure ^{the centre of which} always invariably denotes the surface position of the Inter-tropical Discontinuity (ITD).

As stated at the beginning of this section, the two airstreams dominating the weather over West Africa are the 'south-west monsoon' in the summer months and the dry and dusty northeast trade from the saharan anticyclone in the winter period. The meridional variations in the depth of the southwest monsoon layer is of great importance to the type and intensity of the weather over the region, as the ITD moves from its lowest latitude of 6°N in February to about 23°N in August (Figure 10), following the movement of the sun. Hence the regions surrounding and influenced by the ITD were zoned as A, B, C and D by Hamilton and Archbold (1945), as shown in Figure 11a, relative to the surface position of the ITD and the depth of the moist layer. Details of the weather associated with each zone are given in Figure 11b.

The vertical structure of the monsoon is intricately linked to the dynamics of the flow and is basically governed by the meridional temperature distribution over West Africa. In summer, there is a general poleward temperature gradient from the surface upto about 700hpa. The implied easterly wind shear (or thermal wind) results in the weakening of the south-west monsoon with height and the eventual change into easterlies, leading to the appearance of the so-called African Easterly Jet (AEJ) at the 650hpa level. The moist monsoon depth may reach upto 700hpa in August, considerably weakening

or completely leading to the disappearance of the AEJ and preventing wave and deep convective activity. Figure 11c illustrates the principal components of the West African Monsoon Experiment (WAMEX) and shows the relationship between the ITD, monsoon flow, the jets and the African easterly wave perturbation.

The squall lines and thunderstorms are the most intense products of the interactions between the ITD, AEJ, the monsoon and the easterly wave perturbations. They are virtually the only source of precipitation for the Sahelian subregion of West Africa and whenever they fail to deliver the required rainfall as a result of the failure of the monsoon, we have the attendant disaster - drought.

(c) The Monsoon of East Africa

The East African monsoons, unlike these over India and West Africa, do not result from the differential heating of land and sea surfaces but from the migrations of pressure systems and the associated wind flow patterns following the movements of the sun. The north-south movement of the ITCZ bring, seasonally, two monsoon winds over East Africa.

During the northern summer, the southeasterlies bring into the region a lot of moisture due to their long track over the ocean, although they loose some of this moisture over Madagasca. The western branch of this flow penetrates further inland to form the so-called Congo Air boundary CAB (Figure 12). This south/southwest monsoonflow is part of the large-scale cross-equatorial flow originating as far as 35°S.

It arrives East Africa as a strong current in which is embedded a low-level jet at about 900mb level. The structure and dynamics of this very important jet, together with its influence on East African and West India weather has been extensively discussed (see for example, Findlater, 1977 and HSU (1981)). A five-day oscillation has been observed in the jet stream intensity by Ngara (1977).

The second monsoon winds are the northeast trades - localised called Harmattan over West Africa - which invade East African region during the southern summer, and become northwesterlies on crossing the equator. There are two branches to the flow: a dry continental track over Northern Africa and a moisture-laden track over the Indian ocean and the Arabian Sea.

Because of the above differences in the seasonal monsoon characteristics, East African rainfall is generally bi-modal with two rainy and two dry seasons. The wet seasons are locally known as the 'long' (concentrated within March to May) and 'short' (October to December, in the Southern Summer) seasons. It should be pointed out however, that the ITCZ over the region is rather diffuse at low levels because of local modifying influences, such as orography, many large water bodies (e.g. Lake Victoria) and the Indian Ocean to the eastern Kenyan/Tanzanian coast. These local factors introduce variations into the seasonal rainfall pattern.

Rather surprisingly, it has been observed (Kiangi and Temu, 1984) the Indian ocean monsoon seasons are generally dry periods over the East African region.

3.2 The Easterly Waves

The Easterly wave is one of the best known tropical weather system. First comprehensively studied and documented over the Caribbean by Riehl (1954), it is believed that many of the smaller scale motions (thunderstorms and small lines) are associated with them.

The characteristics and structures of easterly waves are not the same everywhere around the world, even though attempt had been made to apply the same concepts to waves everywhere. The important differences will be brought out clearly here.

(a) Waves in the Caribbean and Pacific

The model of waves in the easterlies as presented by Riehl is shown in Figure 13.

The westward propagation speed of the waves is 5-7 m/s. The wave is weakest at sea-level and increases in intensity upwards to about 600 hPa (4 km) before weakening upwards thereafter. The trade wind inversion is most pronounced about 300 km ahead of the wave through leading to intense subsidence and fine weather. The depth of the moist layer increases rapidly to a maximum at a wave axis.

The Kinematical aspects of easterly waves may be explained from the simplified vorticity equation

$$\frac{d}{dt}(\xi + f) = -(\xi + f)\nabla \cdot \underline{V} \quad \dots (3.2)$$

Since air flows westwards through the wave in the lower layers, the equation implies low-level convergence behind and divergence ahead of the wave axis. The reverse takes place

at upper levels where the basic easterlies are weaker and the wave propagates westwards relative to the flow. Thus the area of active and deep convection and heavy precipitation lies to the rear of the trough.

This model appears to have been applied successfully to the West Pacific waves.

(b) African Easterly Waves

Riehl's model cannot be applied piece-meal to the easterly waves over west Africa and the eastern Atlantic. This is because the wind regimes of the areas differ significantly (compare Figure 14a, b and c for Venezuela, West African and West Pacific regions). The juxtaposition of two tropospheric jets over a rather shallow layer of very moist and warm southerly air is unique and are important over West Africa and the eastern Atlantic. Hence the African Zone of wave activity is unusual when compared to the lower troposphere of the rest of the tropics because temperature changes of 10°C can occur within a latitude band of only 10°; the resulting vertical wind shear leads to the mid-tropospheric African easterly jet (AEJ). The easterly waves develop south of the jet (AEJ) core in a region where the mean zonal flow is barotropical unstable (Burpee, 1972). Wave structure (Figure 15) shows a surface convergence zone only, a cyclonic vortex at 850 mb and a distinct wave pattern at 700 hPa. Wave intensity decreases upwards thereafter. The instability of the

flow has been tested from Charney's (1973) extension of the theory of Charney & Stern (1962) for baroclinic instability. This requires a turning point in the meridional gradient of mean potential vorticity (\bar{q}) which is represented by

$$\frac{\partial \bar{q}}{\partial y} = \frac{\partial}{\partial y} (\bar{\zeta} + f) + \frac{\partial}{\partial p} \left(\frac{p f^2}{R \sigma} \frac{\partial \bar{u}}{\partial p} \right) \quad \dots (3.3)$$

where

$$\sigma = \frac{p}{p_0} \frac{\partial}{\partial p} \ln \bar{\theta}$$

Charney showed that if surface temperature increases northwards, as is the case in northern Africa, then for instability to occur, $\partial \bar{q} / \partial y$ must be negative somewhere in the domain. Some results, due to Resnick (1976) are shown in Figure 4. It is obvious that African waves are due to both barotropic and baroclinic instabilities, with the former ^{the} main contributor.

Figure 16b & c are the vertical profiles of vorticity and divergence in a West Pacific and an East Atlantic wave while Figure 17 shows the distributions of moisture, vertical motion and rainfall amounts around eastern Atlantic waves. There is strongest convergence located ahead of the wave trough where cyclonic vorticity is also strongest. Weather and precipitation distributions are therefore a reverse of the Caribbean situation.

Reed (1984) has suggested from use of spectral analysis of data over East Africa, that another type of rain-bearing wave phenomenon found not at the mid-tropospheric levels as in

West and Central Africa, exists over the East African region. This wave is however not necessarily different from that over central and West Africa.

3.3 The West African Squall Lines

To a large extent, West African squall lines are dependent on or controlled by the summertime monsoon oscillations. They are absent when the monsoon retreats from most parts of West Africa (Nov. - Mar.), suppressed if the monsoon is too deep (giving way to 'monsoon rain' over coastal regions in June/July and very violent when the monsoon depth is about 1-2km especially north of 11°N . However, the variation of the monsoon depth is not the only important factor determining squall line/thunderstorm occurrence. Other basic conditions such as

- (i) the presence of a deep layer of convective or conditional instability
- (ii) a release mechanism for the instability, usually in the form of low-level convergence or topography

must also be satisfied. Even then, propagating convective development is not guaranteed. We shall address this aspect later in this section.

There are two squall line/thunderstorm seasons for regions up to 11°N but only one to the north. The monsoon precipitation in June and, later, the so called 'Little Dry Season' (LDS) of West Africa which affect only coastal areas south of 10°N during July/August both occur between the two storm seasons. Thus, most of the precipitation is from these deep convective systems while the entire rainfall of the sahel comes from the storms. In fact, as has been shown (e.g. Glantz, 1976; Omotosho, 1985) that squall lines and thunderstorms deliver more than 60% of the total annual

precipitation of areas south of 10°N and as much as 80% or more north of this latitude, as shown in Figure 18. Also, their destructive capacity is manifested in the loss of millions of dollars worth of food and cash crops and property by the accompanying strong winds (gusts). The gusts are much stronger north of 11°N for reasons explained later. These convective systems are therefore very important to the socio-economic politics of the region as a whole.

(a) Mechanisms of Storm Development and Sustenance

Several researchers have attributed squall line formation to different mechanisms. It was initially believed that orography played a major role in their initiation and alignment (e.g. Barreiros, 1964) until Omotosho (1984) showed that although these physical features do influence the intensity of the storms, the storms do not, in general, owe their existence to orography. Later and even presently, the propagating storms are regarded as the products of low-level convergence associated with the synoptic-scale easterly waves in areas where the atmosphere is convectively or conditionally unstable (see for example, Reed et al (1979) and Adefolalu (1985)) because they occur during the period (May - Sept) of wave activity. Figure 18b shows squall lines are found almost anywhere on the easterly wave although mostly ahead of the wave trough. Also, Omotosho (1981), McBride & Gray (1980) have demonstrated that the waves only have a modulating but not a forcing effect on deep convection over the GATE area.

Notwithstanding all these, it is to be emphasised that the release mechanism is a crucial stage in thunderstorm development. The required low-level convergence usually manifests

itself as cyclonic vortices or convergence lines (often as asymptotes of convergence) at the 900 or 850hpa level. When the vortices are accompanied by easterly waves at the 700hpa level, the depth of convergence increases and hence upward motion is greatly enhanced. Vigorous thunderclouds result especially if the convective available potential energy (proportional to the buoyancy of the in-cloud rising air parcel) is large. This is the perceived role of the easterly perturbation.

So what is/are the forcing mechanisms for thunderstorms and squall lines? The answer(s) to this question has (have) not yet been fully uncovered despite the extensive research on them. However, it is now very evident that the existence of a mid-tropospheric wind maximum, the AEJ, with reversed shear in the lower levels is important to their development (Moncrieff & Miller (1976); Bolton (1981)). The systems are in quasi-steady state with the density current (gust front) feeding the cloud cells with warm and moist (high θ_e) air of the monsoon, as shown in Figure 19. It is also suggested that the simultaneous presence of positive boundary layer vertical wind shear, a moist layer of at least one kilometre depth and a distinct and organised AEJ are all necessary conditions for widespread thunderstorms to develop and be aligned into a line (see, for example, Figure 20). Most recently, Omotosho (1987) has found that the storms occur most frequently when boundary layer Richardson Number Ri is within the range $-2 \leq Ri \leq 0$ and also $1 \leq Ri \leq 4$ in the middle troposphere.

The interaction between the clouds, gust front and the boundary layer is essentially that of the Conditional Instability of the Second Kind (CISK). Such interaction is possible only because of the peculiar regime over West Africa which causes the relative flow to enter the storm clouds from the front. The storm cloud sucks in cool, dry (low θ_e) air from the front in the layer 800 - 600hpa and becomes the evaporative downdraft due to the drag of the falling precipitation. Some of the precipitation is evaporated into the down-draft which is cooled and then reaches the surface as strong gusts of wind. Because of the large temperature contrast and wind shifts across the boundary of this cold downward rushing air and the very warm, moist ambient (high θ_e) air at and close to the ground, a frontal zone (gust front) is formed. The warm, moist boundary layer air is thus forced upward into the cloud. This way the storms are assured of the much needed moisture and hence the accompanying latent heat release. The precipitation into the large-scale flow then enhances the moisture convergence at the gust front and the continued sustenance of the storms until the front travels too far ahead of the storm cloud. At this stage, the moisture supply (and hence latent heat) is drastically reduced or cut-off and the storm begins to decay.

(b) Squall-line Movement

Unlike their initiation, the mechanisms for squall line movement is now reasonably well understood. The vital roles played by the vertical transfer of (horizontal) momentum, termed evaporative downdraft, and the AEJ are well accepted; so also is the requirement of a relatively deep layer of dryer air between 800-600hpa. Moncrieff and Miller (1976) have shown that the AEJ, U_j , and the energy stored in the convectively unstable layer (CAPE) are related to the squall propagation speed, C_s as

$$C_s = U_j + 0.3\sqrt{\text{CAPE}} \quad \dots (3.3)$$

CAPE is proportional to the positive area on the Tephigram. However, Omotosho (1983) showed that although the above expression gives reliable values, the determination of CAPE is a rather cumbersome process and is therefore not operationally very helpful. A new predictive but empirical expression was proposed for some Nigerian station (Minna and Kano) as

$$C_s = aU_j + b\sqrt{\Delta T} \quad \dots (3.4)$$

a and b are constants which are distinct for each station and are obtained from the stations data:

$$\sqrt{\Delta T} = (T_s - T_j) / T_s \quad \text{where } T_s \text{ and } T_j$$

are surface temperature about 2-3 hours before squall arrival and jet-level (700hpa) temperature appropriate to arrival time, respectively.

Notice that the two expressions are functionally similar but (3.4) explicitly relates the boundary and mid-tropospheric layers together. Also, the equation can be used to estimate the maximum gust expected from any squall line, thus allowing warnings to be given to the public and relevant organisations such as the Navy, Airforce, Airways and Electricity companies. Furthermore, ΔT is obviously an easy quantity to evaluate. All these therefore make the expression advantageous and operationally more useful.

Similar expressions to (3.4) above can easily be obtained for any West African radiosonde station. However, the time limit for prediction is too short and a way must be found to predict surface temperatures at least six hours ahead for the method to be more versatile.

(c) Comparison with Squall line of Other Regions

West African squall lines are similar, in many respects, to their counterparts over Venezuela although they occur within dissimilar flow regimes. They all propagate through, and in general travel faster than

the basic flow at all levels in the convective cloud layer as evident from equations (3.3) and (3.4); this properly causes inflow of air into these systems from the front. This is in contrast to mid-latitude squall lines which are advected since they travel at nearly the mean wind speed in the cumulonimbus layer.

Again, unlike temperate squall lines, tropical ones are associated with larger values of the Richardson number, Ri while tropical storms are characterised by values of Ri greater than 2.0 in the convective layer, temperate latitude storms are associated with lower Richardson number ($Ri \leq 1.0$, high wind shear). The transfer of momentum in tropical storms of Venezuela and West Africa are distinctive and of large magnitude. Also, their propagation speed (C_s) is almost constant over a wide range of the Richardson Number.

3.4 Tropical Cyclones

As nature's most destructive weather systems, tropical cyclones represent a special class of intense atmospheric vortices. Although there is as yet no universal agreement about the processes which lead to the transformation from tropical disturbances to cyclones, Gray and his group at Colorado State University (Gray 1979, McBridge 1979) have carried out extensive observational studies on the systems. They suggest that tropical cyclones develop in regions where

- (a) there is a non-zero value of the Coriolis parameter
- (b) the sea surface temperature $> 26.5^\circ\text{C}$
- (c) there is higher than normal ~~relative~~ humidity
- (d) there is zero or negligible vertical wind shear near the centre of the system
- (e) a weak warm-core system with a low-level cyclonic circulation having a high value of relative vorticity on the scale of about 500-800km exists and the vorticity falls off with height.

The temperature constraint is necessary to maintain a saturated adiabatic lapse-rate throughout the troposphere with a tropopause temperature of -78°C (Pearce, 1981).

The origins and areas affected by cyclones are depicted in Figure 22a while Figure 22b shows the latitudes of their initial detection. The latter figure shows that cyclones do not form $4-5^\circ\text{C}$ from the equator, are most favoured in the latitude belt $5-20^\circ\text{C}$, and are most frequent in the North West Pacific.

In a tropical cyclone, the balance of forces is between the centrifugal force of winds rotating at speeds greater than about 50m/s and the pressure gradient force over a horizontal scale of about 100km. Motion is in hydrostatic balance and there are large temperature deviations.

A tropical cyclone has a well-defined central region - the eye - whose formation depends on the angular momentum of an annular ring of rotating air as:

$$V_\theta r = \text{constant} \quad \dots \quad (3.7)$$

where V_θ is the tangential velocity and r the radial distance from the centre. As the centre of the storm is approached (r decreases) the tangential velocity increases. But since the cyclone kinetic energy is finite, the wind cannot increase indefinitely and it thus tends to spiral upwards round a central region of calm subsiding motion. Figure 23 is a typical vertical cross-section across a tropical cyclone. The eye is warmer than its environment throughout its depth, making tropical cyclones warm-core systems.

Cyclone genesis would seem to depend on the strength of low-level cyclonic and upper tropospheric anticyclonic circulations. Their genesis may be thought of from the conditions which lead to an increase in the absolute angular momentum, M_a , within a cylindrical area of the disturbance region out to about 6° radius.

This can be represented by:

$$\int \frac{\partial M_a}{\partial t} \delta M = - \int_0^R \int_0^{2\pi} \frac{V_r M_a}{g} \delta \theta \delta p + \int r F_\theta$$

where

$$M_a = V_\theta r + \frac{1}{2} f r^2$$

and

$$\int \delta M = \int_0^R \int_0^{2\pi} \int_0^{p_s} \frac{r}{g} \delta r \delta \theta \delta p$$

V_r, V_θ, p_s represent radial tangential winds and surface pressure respectively.

The term on LHS is the mean rate of change in momentum within the disturbance. The first term on the right represents the import of momentum at the 6° radius boundary into the region; the last term is the momentum dissipation. Observational results have indicated that there is a much value of second over last term in (3.8).

The difference between the relative vorticity at lower and upper troposphere, the so-called genesis potential, is also an important factor. Developing cyclones are found to be characterized by large differences.

This difference is concentrated in the lower and upper troposphere as shown in Figure 24.

Cyclone intensification have mostly been modelled on the CISK theory. While the theory appears to give satisfactory explanation of the later stage and inner-core region intensification, it does not explain how the deep cyclone from which integrations started is itself formed.

Much further modelling assisted by results from observational study are still required before cyclone understanding and prediction can be fully achieved.

4. BOUNDARY PROGRESS AND SURFACE ENERGY BUDGET

In section 1.4, the radiative processes and energy balance were discussed. This balance may be expressed as:

$$Q = Q_H + Q_E + Q_G \quad (4.1)$$

where Q_H and Q_E are the sensible and latent heat fluxes out of the surface and Q_G the flux into the ground. Q (the basic input of surface energy budget) is the net radiation absorbed by the ground as a consequence of which its temperature changes according to time of the day (see Figure 25). When energy storage, ΔQ_s in the layer (or volume) is considered, (4.1) becomes:

$$Q = Q_H + Q_E + Q_G + \Delta Q_s \quad (4.2)$$

These equations express the concept

$$\text{Energy Input} - \text{Energy Output} - \text{Storage} = 0$$

Three possibilities exist:

- (a) Input > Output \Rightarrow flux convergence ($\Delta Q_s > 0$)
- (b) Input < Output \Rightarrow flux divergence ($\Delta Q_s < 0$)
- (c) Input = Output ($\Delta Q_s = 0$).

The temperature of a layer of air near the ground can be changed by the convergence or divergence of one or more of Q_s , Q_E and Q_G (horizontal flux). If the site is assumed free of horizontal advection and the air remains unsaturated, then only Q and Q_H effect the change in the air temperature. Hence the atmosphere is warmed by day when Q_H is directed upwards and vertical turbulence mixing is efficient with remaining effectively constant with height. The right situation is that Q_H is directed into the ground and the air is cooled by the vertical divergence of Q_H ($-\Delta Q_H$). Up to about 50m above the ground variations in radiatively-important agents (water vapour, CO_2 , dust) is negligible; this is the constant-flux layer.

The rate of heat flow into and out of the soil depends on the temperature gradient and the soil characteristics, so that the flux-gradient relationship is:

$$Q_G = -k_s \frac{\partial T}{\partial z} \quad (4.3)$$

where k_s is the thermal conductivity ($\text{W m}^{-1} \text{K}^{-1}$); it is not strictly a constant as it varies with depth and time. Thus by day time when $\partial T / \partial z$ is negative, Q_G is positive into the air (i.e. a surface energy loss). The general diurnal and seasonal cycles of soil temperature at different depths are shown in Figure 26a and b while Figure 26c is for a tropical continental station (Ile-Ife, Nigeria). The heat wave penetrates to lower depths with decreasing amplitudes and the maximum and minimum temperatures are time-lagged. Both features are dependent on the thermal diffusivity $k_s (= k_s / C_s)$ is the thermal capacity

The wave amplitude at any depth $(\Delta T_s)_z$ decreases exponentially with time as:

$$(\Delta T_s)_z = \Delta T \exp[-z(\pi/k_s P)] \quad (4.4)$$

where P is the wave period.

The method of estimating heat flux Q_G is to use heat plate of known conductivity since the variability of k_s renders equation (4.3) impracticable. The plates are usually buried horizontally and at least 10mm below the soil surface. The temperature gradient across, and the heat flux through, the plate (and hence the soil) are proportional to the output of the plate as measured by the connected thermopile. Due to the plate's closeness to the surface, over - (or under -) estimation may occur. This is accounted for by subtracting (adding) the change in heat storage (ΔQ_s) in the overlying layer.

A similar equation to (4.3) is also valid for the flow of water, M_v from the soil:

$$M_v = -\rho k_w \frac{\partial \bar{q}}{\partial z} \quad (4.5)$$

where ρ is air density, k_w the molecular diffusivity for water vapour ($\approx 0.20 \text{ m}^2 \text{ s}^{-1}$) and q is the specific humidity.

Equations (4.3) and (4.5) are strictly valid in the soil or laminar boundary layer but not in the atmosphere where convective activity dominates and real molecular transfer is negligible. Despite this, the analogy of the roles of molecules in conduction can be extended to that played by eddies in convection. The transfer of horizontal momentum in the laminar boundary layer is given by:

$$\tau = \rho k_m \frac{\partial \bar{u}}{\partial z} \quad (4.6)$$

where τ is the shearing stress (force per unit area) to the kinematic viscosity ($\approx 0.15 \times 10^{-4} \text{ m}^2 \text{ s}^{-1}$), \bar{u} the mean wind. The analog for the turbulent surface layer above this laminar layer is

$$\tau' = \rho K_m \frac{\partial \bar{u}}{\partial z} \quad (4.7)$$

where K_m is the eddy viscosity ($\text{m}^2 \text{ s}^{-1}$). K_m is about 5 orders of magnitude greater than k_m .

The study of momentum exchange is important because it is central to studies concerning transports of heat Q_H and moisture Q_E and also to pollutant dispersal.

Under conditions of neutral stability, the variation of wind with height is given by the logarithmic wind profile equation:

$$\bar{u} = \frac{u_*}{k} \ln \left(\frac{z}{z_0} \right) \quad (4.8)$$

where \bar{u} is the wind speed at height z , u_* ($u_*^2 = \tau/\rho$) is the friction velocity, k the von Karman's constant (0.40), and z_0 is the roughness length (m). Since u_* can be evaluated from wind profile measurements (slope is k/u_* from (4.8)) the stress τ can be obtained which can then be used for evaluating other fluxes.

The above discussion relates to neutral conditions where buoyancy is unimportant, as in cloudy skies and strong winds. In such situations forced convections due to frictionally-generated eddies dominate. In unstable conditions momentum, heat and moisture exchanges are enhanced, although forced convection are still dominant near the ground up to say about 2m. Above this level, free convection becomes dominant and stability effects on vertical exchanges increases, Figure 27 gives the wind

profiles under different stability conditions. Vertical wind gradients are largest under stable situations and weakest in an unstable atmosphere.

4.1 Heat and Moisture Fluxes

The sensible heat Q_H passing through the laminar boundary layer by molecular conduction is:

$$Q_H = -\rho c_p k_H \frac{\partial \bar{T}}{\partial z} \quad (4.9)$$

and the flux of sensible heat in the overlying turbulent layer is given by

$$Q_H' = -\rho c_p K_H \left(\frac{\partial \bar{T}}{\partial z} - \bar{q} \right) \quad (4.10)$$

or, in terms of potential temperature θ

$$Q_H' = -\rho c_p K_H \frac{\partial \bar{\theta}}{\partial z} \quad (4.11)$$

K_H is the eddy heat conductivity ($\text{m}^2 \text{ s}^{-1}$). The vertical transport of sensible heat is typicalised in Figure 28 which shows the correlation between stability, temperature and the heat flux. Large upward heat transfer and high temperature are associated with unstable conditions (w positive).

Evaporation from the surface through the laminar sub-layer is given by equation (4.5). The flux of the water vapour in the turbulent layer is:

$$E = -\rho K_w \frac{\partial \bar{q}}{\partial z} \quad (4.12)$$

and the latent heat flux Q_E is

$$Q_E = -\rho L K_w \frac{\partial \bar{q}}{\partial z} \quad (4.13)$$

where K_w is eddy diffusivity and L the latent heat of vaporisation.

The exchange of moisture between surface and the atmosphere determines the humidity. In contrast to the heat flux which is upwards by day and downward towards the surface during the night, water vapour flux is predominantly upwards. Although water may return to the surface as dew under certain conditions, this is almost negligible compared to the daytime flux.

Figure 28 shows that the vertical transfer of sensible heat is correlated with the upward motion. The flux of a quantity χ with fluctuations χ' about its mean can thus be expressed as:

$$F_\chi = \rho \overline{w' \chi'}$$

where the overbar may be time or space average. Therefore sensible and latent heat fluxes may be given as:

$$\begin{aligned} Q_H &= \rho C_p \overline{w'T'} \\ Q_E &= \rho L \overline{w'q'} \end{aligned} \quad (4.13)$$

However, instrumental response to turbulence is a great problem especially near the ground and this direct method of flux estimation is not widely used. With the present technological advance, there is great hope of applying this simple straightforward technique which is independent of nature of the surface (roughness) and stability.

The profile method, which is commonly used, is based on the assumption of $K_H = K_M = K_M$. In such cases, the ratios of the fluxes are:

$$Q_H / Q_E = \frac{C_p}{L} \frac{\Delta \bar{\theta}}{\Delta \bar{q}} \quad (4.14a)$$

$$Q_E / \tau = -L \frac{\Delta \bar{q}}{\Delta \bar{u}} \quad (4.14b)$$

Even if the assumption was not made, a knowledge of the behaviour of, say, K_M / K_H would still allow the above method.

There are two techniques under the profile method - the aerodynamic and Bowen ratio methods. The aerodynamic method is strictly valid for neutral conditions only under the assumption of steady-state, invariant fluxes with height and constant K_s .

With these the various fluxes are estimated. With $\frac{\partial \bar{u}}{\partial z} = \frac{u_*}{kz}$ from (4.8), they are given by:

$$Q_H = -\rho C_p k^2 z^2 \left(\frac{\Delta \bar{u}}{\Delta z} \cdot \frac{\Delta \bar{\theta}}{\Delta z} \right) \quad (4.15a)$$

$$Q_E = -\rho L k^2 z^2 \left(\frac{\Delta \bar{u}}{\Delta z} \cdot \frac{\Delta \bar{q}}{\Delta z} \right) \quad (4.15b)$$

The Bowen ratio method has the advantage of being stability-independent. The Bowen ratio β is given by

$$\beta = \frac{Q_H}{Q_E} = \frac{C_p}{L} \frac{\Delta \bar{\theta}}{\Delta \bar{q}} \quad (4.16)$$

so that from the surface energy balance equation (4.1), the fluxes can be written in terms of β as

$$Q_H = \beta(Q - Q_a) / (1 + \beta) \quad (4.17a)$$

$$Q_E = (Q - Q_a) / (1 + \beta) \quad (4.17b)$$

The partitioning of the energy over different surfaces at various locations are shown in Figure 29.

Further discussion of measurements is done under "Satellite Meteorology".

References

1. Adefolalu, D.O. 1974: On Scale interaction and lower tropospheric summer easterly perturbation over tropical West Africa. Ph.D. Thesis, Department of Meteorology, Florida State University, U.S.A.
2. Adefolalu, D.O. 1985: Further aspects of Sahelian Drought as evident from Rainfall Regime of Nigeria. Arch. Met. Geoph. & Bioc., Ser. B36, 277-295.
3. Adejokun, J.A. 1966: The Three dimensional structure of the Inter tropical Discontinuity over Nigeria. Techn. Note No. 39, Nigerian Meteorology Department, Lagos.
4. Babatunde, E.B. and Balogun, E.B. 1983: The diurnal temperature variation near the ground surface at a tropical station, Nigerian Meteorology Journal, 2, 65-82.
5. Barrefors, B.B. 1964: Disturbances in West Africa as Gravity waves in the Intertropical discontinuity surface. Tech. Note on No. 29, Nigerian Met. Dept., Lagos.
6. Burpee, R.W. 1972: The origin and structure of easterly waves in the lower troposphere of North Africa, J. Atm. Sci., 29, 77-90.
7. Charney, J.G. 1947: The dynamics of long waves in a baroclinic westerly current in J. Meteorology, 4, 135-162.
8. Charney, J.G. and Eliassen, A. 1964: On the growth of the hurricane depression J. Atm. Sci., 21, 159-172.
9. Charney, J.G. and Stern, M.E. 1962: On the stability of internal baroclinic jets, J. Atm. Sci., 19, 159-172.
10. Charney, J.G. 1967: The Intertropical Convergence Zone and the Hadley circulation of the atmosphere. WMO/IUGG proceedings on Numerical Weather Prediction Tokyo.
11. Eady, E.T. 1949: Long waves and cyclone waves. Tellus 1, 33-52.

12. Findlater, J., 1977: Observational aspects of the low-level cross-equatorial jetstream of Indian Ocean. *Rure App. Geophy.*, 115, 2151-2262
13. Glantz, M.H. 1976: Value of a reliable long range climate forecast for the Sahel: A preliminary Assessment, IFIAS commissioned study Report.
14. Gray, W.M. 1979: Hurricanes: their formation, structure and likely role in the tropical circulation. In "Meteorology Over Tropical Oceans".
15. Hamilton, R.A. and Archbold, J.W. 1945: Meteorology of Nigeria and adjacent territory. *Quart. J. R. Met. Soc.*, 71 245-262.
16. Hau, 1981: Interactions between meso-scale and synoptic-scale wave under the influence of wind systems in Somali. *Intern. Conf. on Results of Monsoon Experiments.*
17. Holton, J.R. 1972: An Introduction to dynamic meteorology Academy Press.
18. Houze, R.A. 1977: Structure and dynamics of a tropical Squall-line system. *Mon. Wea. Rev.*, 105, 1540-1567.
19. Kiangi, P.M.R. and Temu, J.J., 1984: Equatorial Westerlies in Kenya - Are they always rain laden? *Ibid.*, 144-146.
20. Lettau, H. 1956: Theoretical notes on the dynamics of equatorial atmosphere *Beitrag zur Physik der Atmosphere*, 29, 107.
21. Lockwood, J.G. 1974: World Climatology: An environmental Approach. Fletcher & Son Ltd., Norwich, Britain.
22. Lorenz, E.N. 1967: The Nature and theory of the General Circulation of the atmosphere W.M.O Nos 218 TP 115, Geneva.
23. Moncrieff, E.W. and Miller, E.J 1976: The dynamics and simulation of tropical cumulonimbus and squall lines *Quart. J. R. Met. Soc.*, 102, 373-394.
24. Ngara, T. 1977: Some aspects of the East African low-level Jet. M.Sc Thesis. University of Nairobi.
25. Obasi, G.O.P., 1984: Drought in Africa. WMO. WCP Newsletter No. 6.
26. Omotosho, J.A., 1981: A theoretical and observational study of cumulus clouds and their meso-scale environment. Ph.D Thesis, Dept. of Met., University of Reading, U.K.

27. Omotosho, J. Bayo 1983: Prediction of maximum gusts in West African line squalls. *Nigerian Met. Journ.*, 1, 94-100.
28. Omotosho, J. Bayo, 1984: On the Initiation and Organisation of deep convective systems over West Africa. *WMO Conference on GATE 4 WAMEX. Dakar, 154-157.*
29. Omotosho, J. Bayo, 1984: Spatial and Seasonal variations of line squalls over West Africa. *Arch. Met. Geoph. Biocl.*, Ser. A33, 143-150.
30. Omotosho, J. Bayo, 1985: The separate contributions of line squalls, Thunderstorms and the monsoon to the Total Rainfall in Nigeria. *Journ. of Climatol.* 5, 543-552.
31. Omotosho, J. Bayo, 1987: Richardson number, vertical wind shears and storm occurrences at Kano, Nigeria. *Atmospheric Research Elsevier, The Netherlands.* (in print).
32. McBride, J.L and Gray, W.M. 1980: Mass divergence in tropical weather systems. Part II: Large-scale controls on Convection. *Quart. J.R. Met. Soc.*, 100, 23-38.
33. Pearce, R.P., 1978: On the concept of available potential energy. *Quart. J.R. Met. Soc.*, 104, 737-755.
34. Reed, R.J. Payne and McGarry, 1979: Unpublished Manuscript.
35. Riehl, H., 1979: Climate and Weather in the Tropics, Academic Press, New York.
36. Resnick, F.A., 1976: The generation of African waves, *J. Atm. Sci.*, 33, 1955-1969.

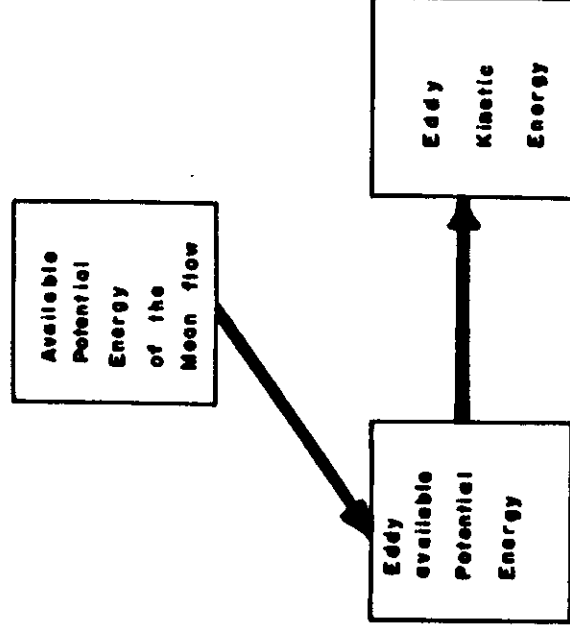


Fig. 1a Direction of Energy flow in an amplifying baroclinic wave.

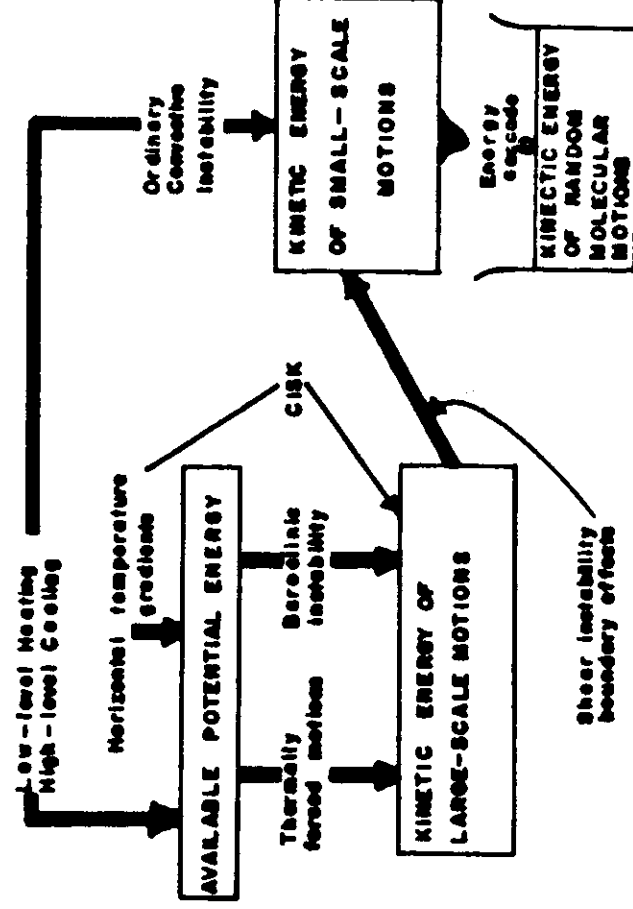


Fig. 1b Kinetic energy cycle scheme in atmospheric general circulation
(From Wallace & Gobe, 1977)

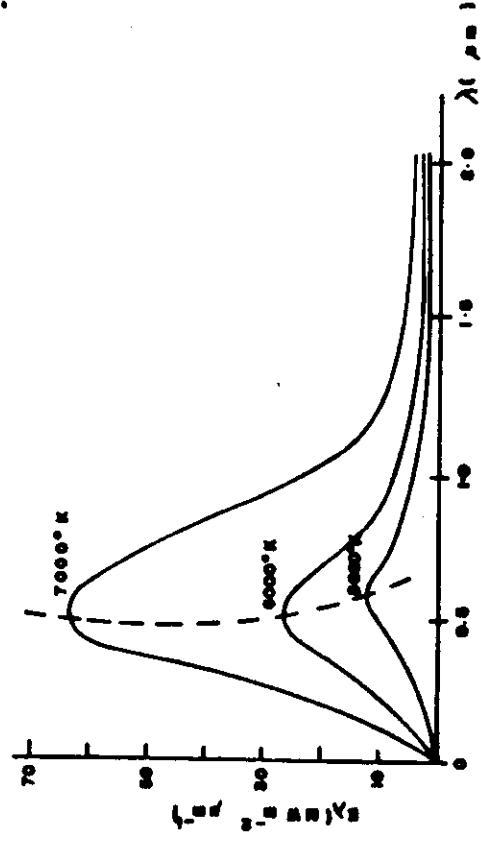


Fig. 2a Black-body emission at indicated temperatures.

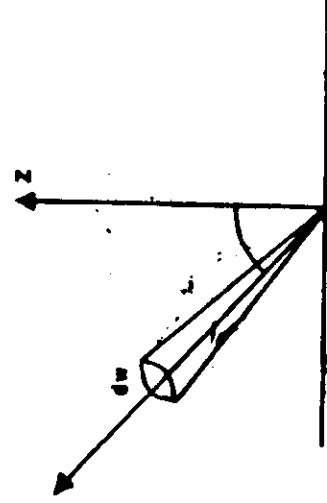


Fig. 2b The solid angle

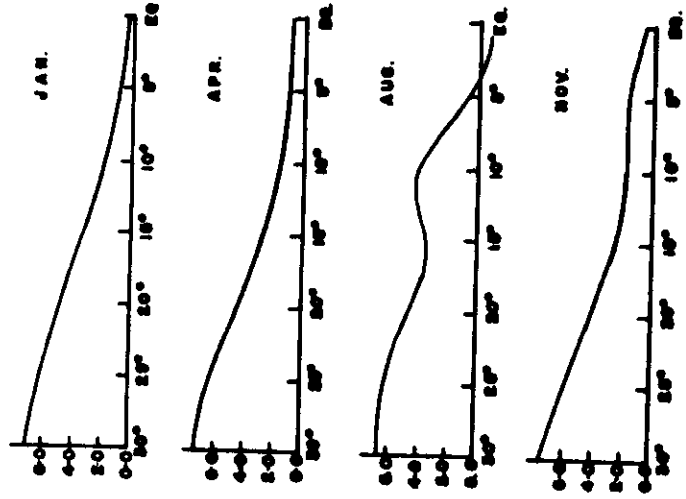


Fig. 3. Absolute vorticity ($\times 10^{-5} \text{ s}^{-1}$) versus latitude at 5°E , 700 mb

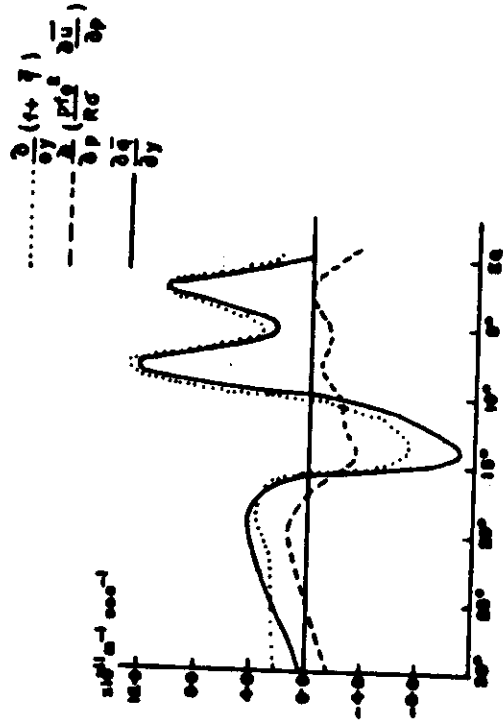


Fig. 4. Gradient of pseudo-potential vorticity versus latitude at 5°E , 700 mb

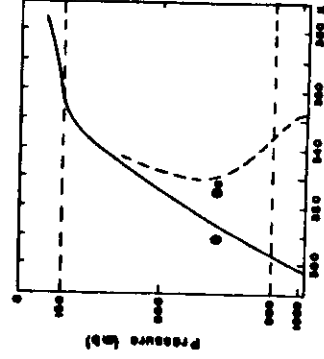


Fig. 5. Typical sounding in the atmosphere showing the vertical profiles of potential temperature θ , equivalent potential temperature θ_e (adopted from Holton, 1972)

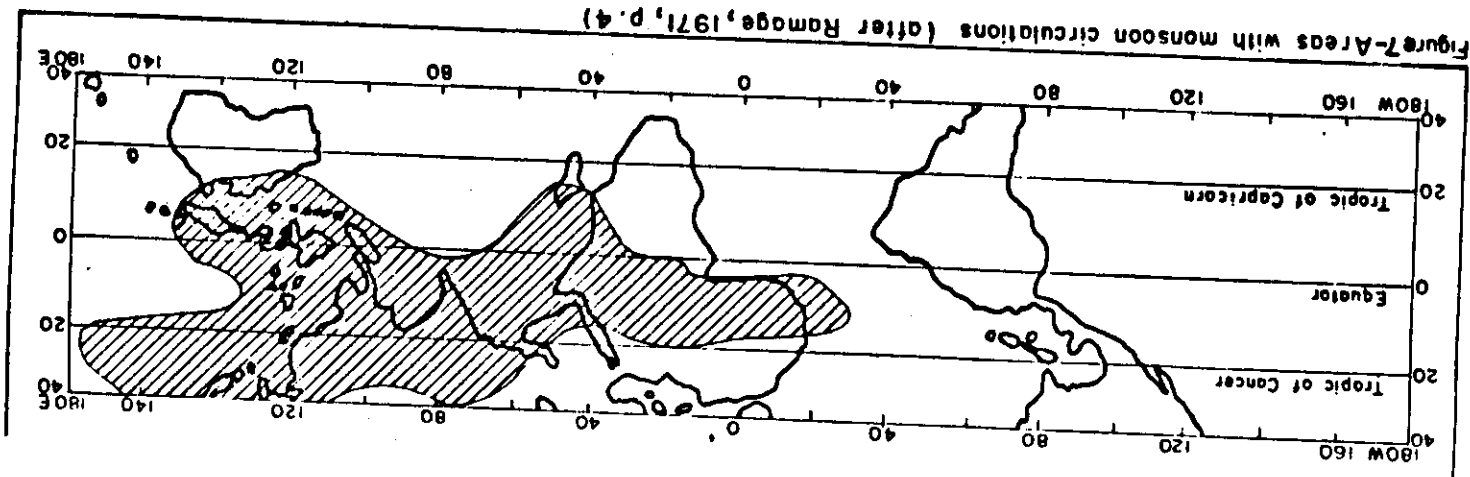
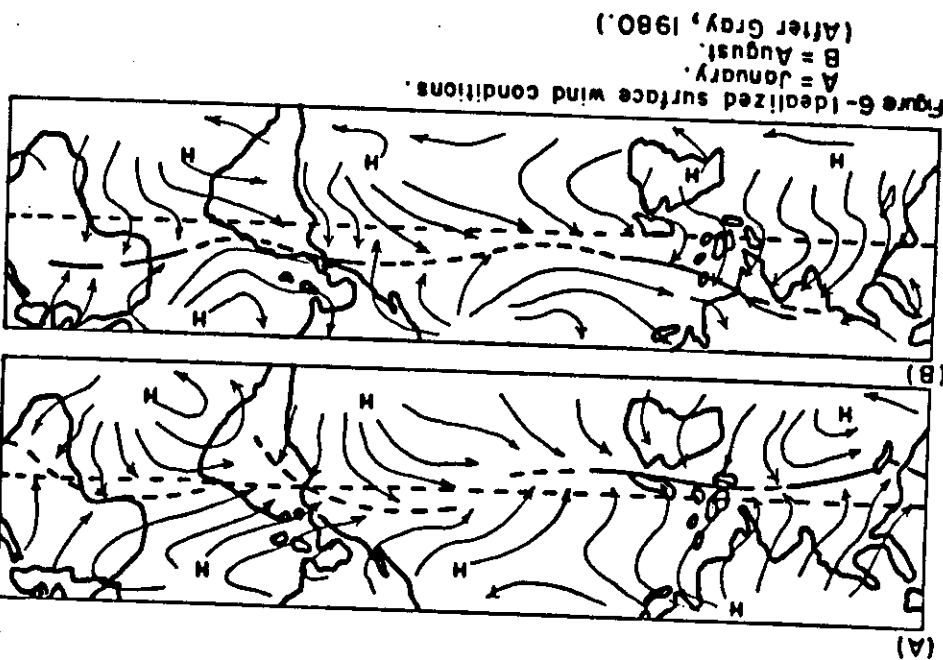
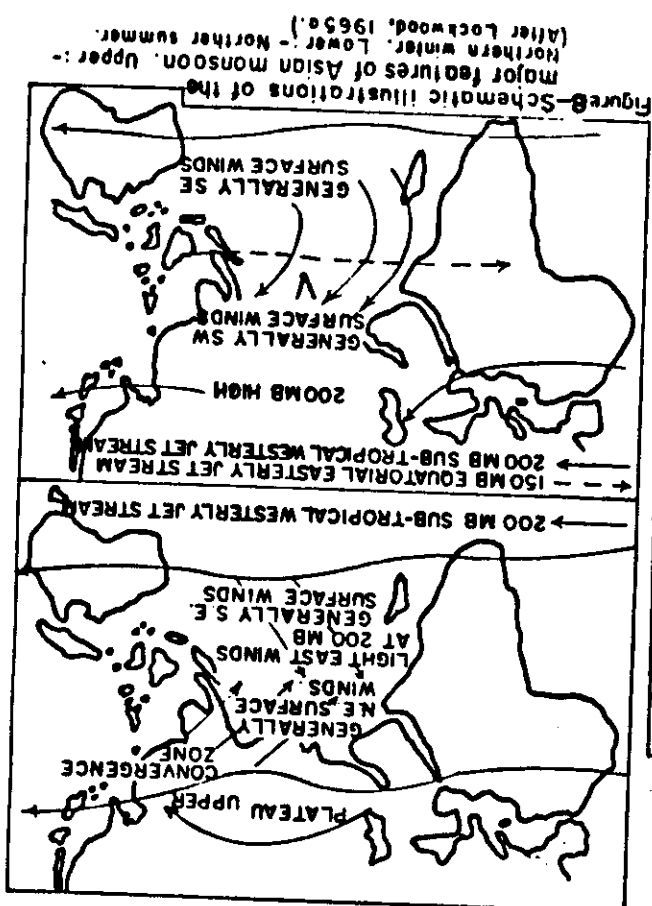


Figure 7-Areas with monsoon circulations (after Ramog, 1971, p. 4)

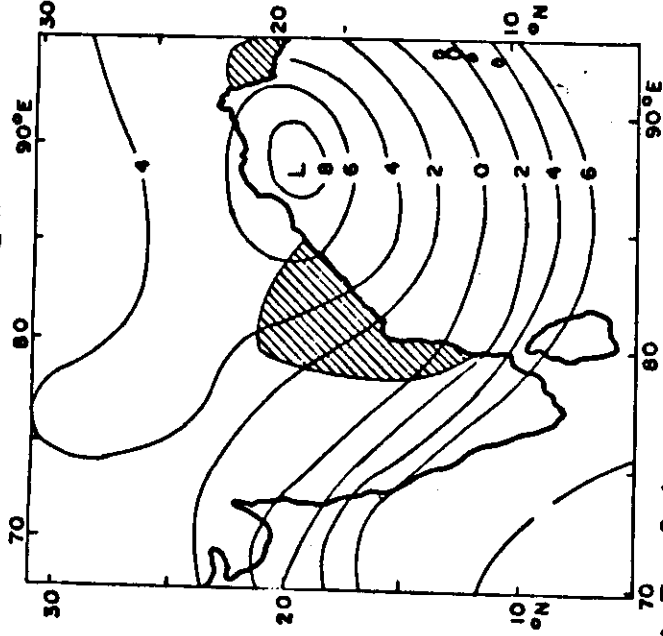


Figure 9a—An example of a monsoon depression over the Bay of Bengal. 1000-mb contours in decimetres for 12 00 GMT on August 20th, 1967. Hatched areas: Continuous rainfall. (Adapted from Nicuwell, 1977).

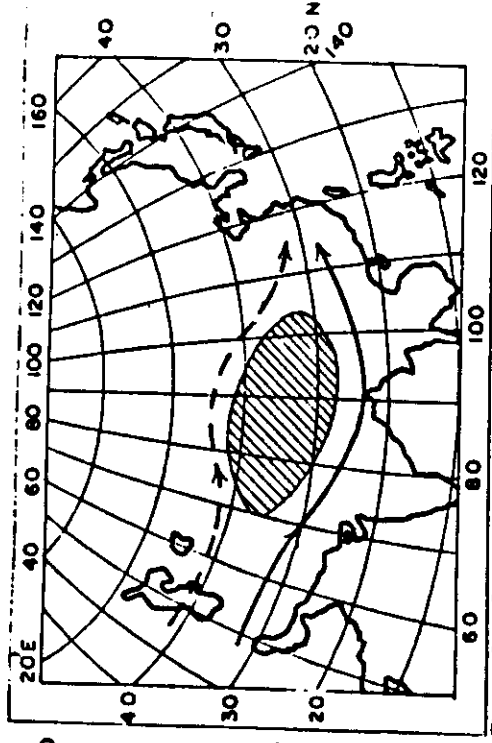


Figure 9b—Change in flow pattern in upper atmosphere resulting from displacement of sub-tropical westerly jet stream to the north of Himalayas.

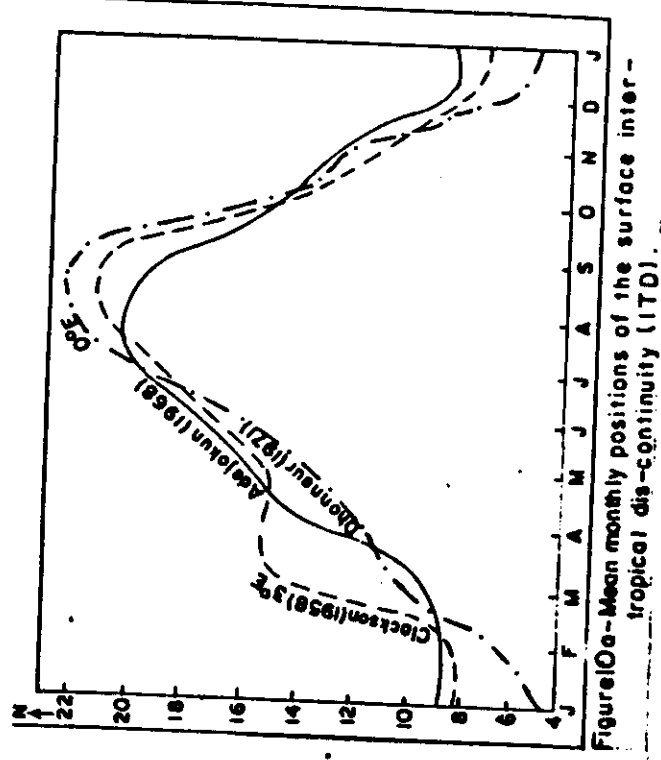


Figure 10a—Mean monthly positions of the surface inter-tropical discontinuity (ITD).

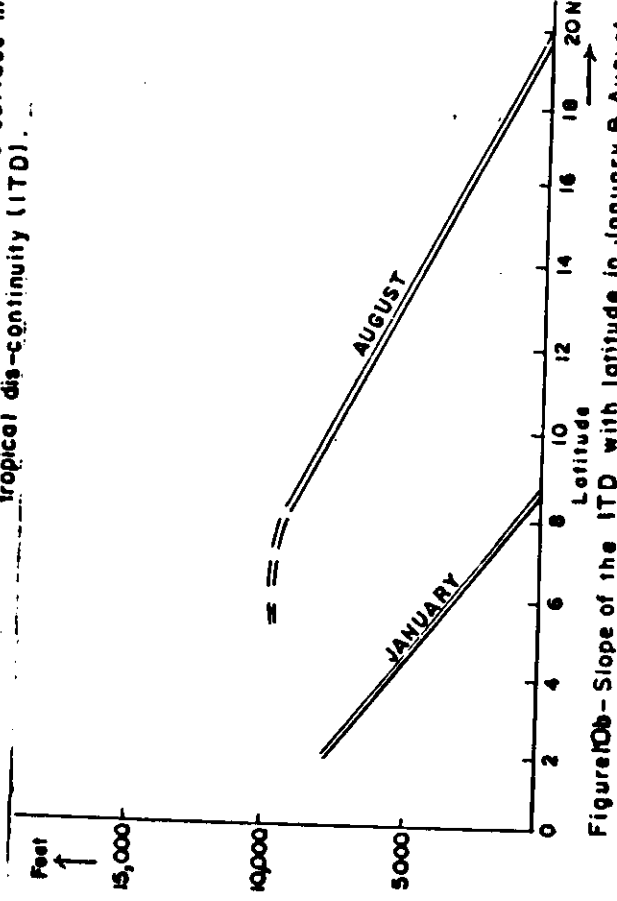


Figure 10b—Slope of the ITD with latitude in January and August.

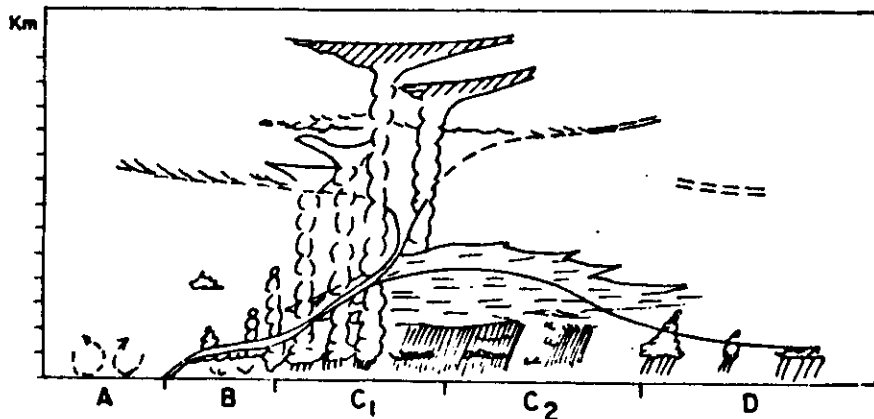


Figure 11a - Vertical cross-section across the ITD over West Africa

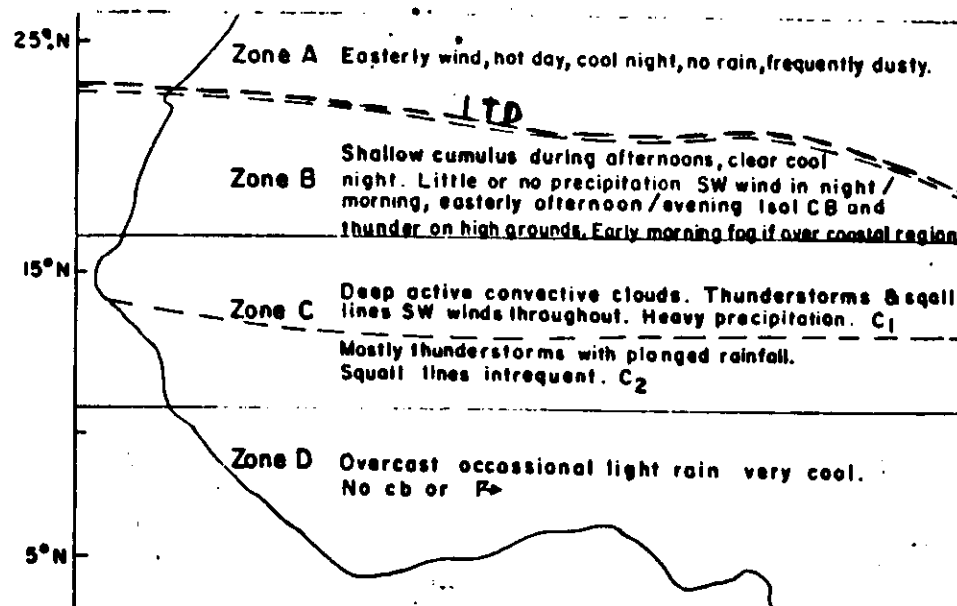


Figure 11b - ITD position and weather distribution in August.

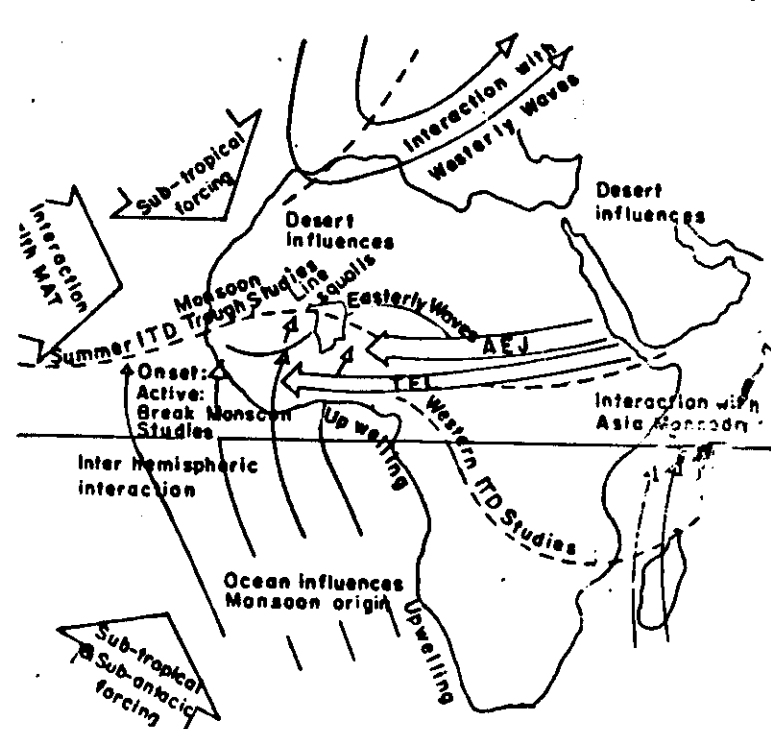


Figure 11c - Schematic illustration of the overall distribution of the main components of WAMEX.

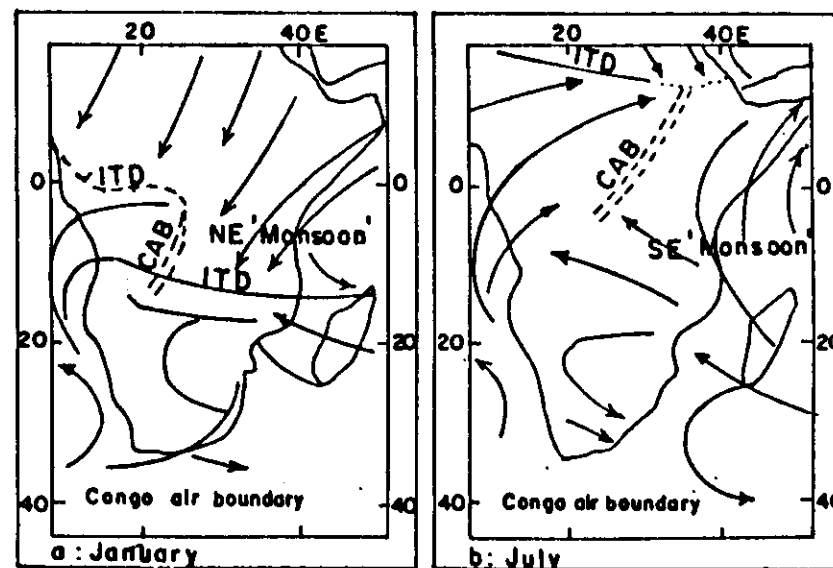
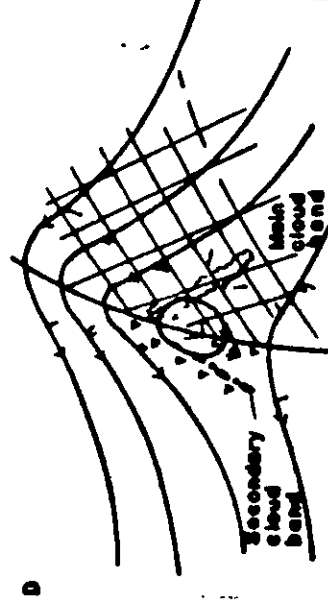
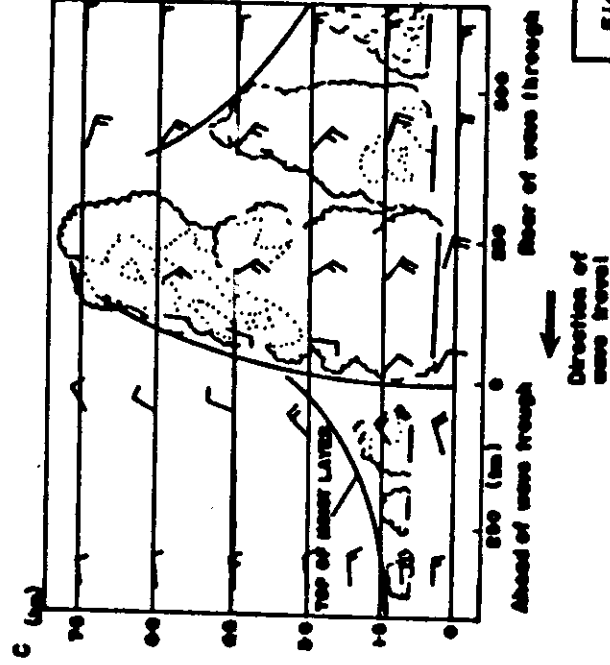
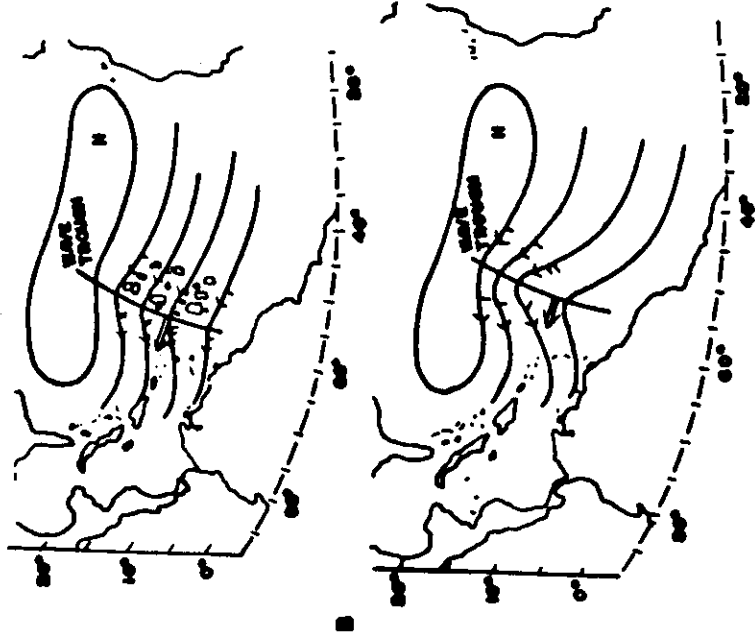


Figure 12 - Features of the East African and Congo Monsoons.



D: Vertical cross-section from west (left) to east (right). Cloud forms are shown schematically and not to scale.

E: Schematic picture of a very deep easterly wave, showing streamlines and major cloud bands.

Fig. 15- Schematic illustrations of major features of 'easterly wave' type of tropical disturbances.

A: Surface streamlines of weak-to-moderate amplitude wave, which typically moves westward in direction of heavy arrow at a speed slightly slower than prevailing trade-wind. The area of cloudiness and rain is commonly found to the rear of the trough.

B: 500 mb streamlines pattern in typical moderate easterly wave.

Comparison of Wind Profiles

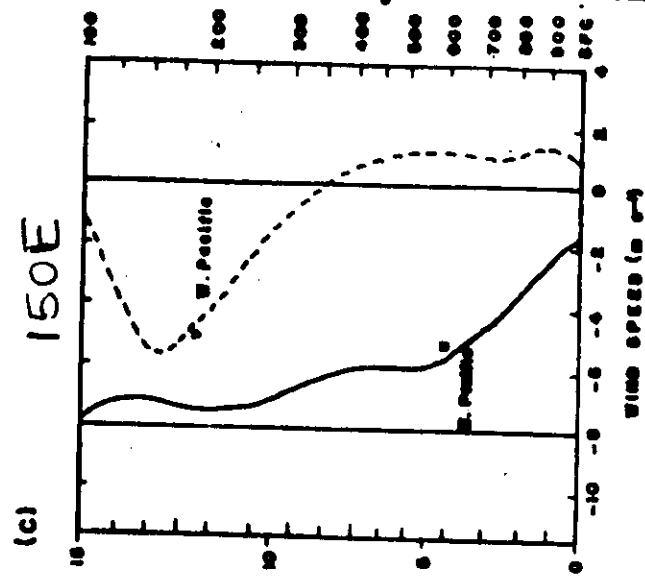
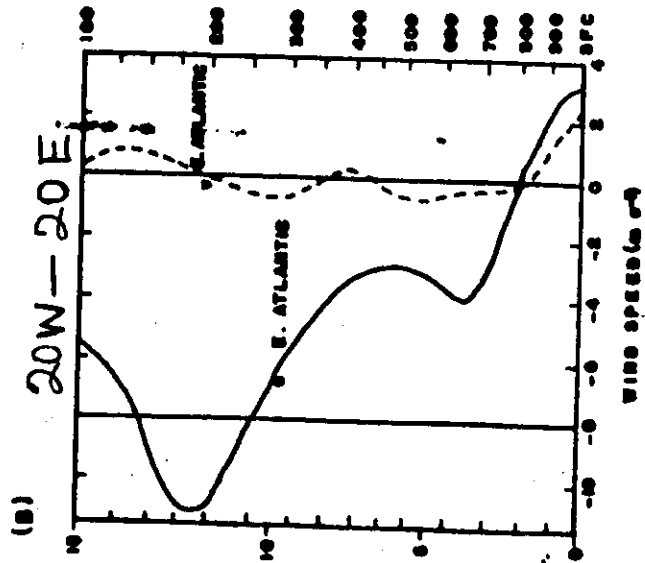
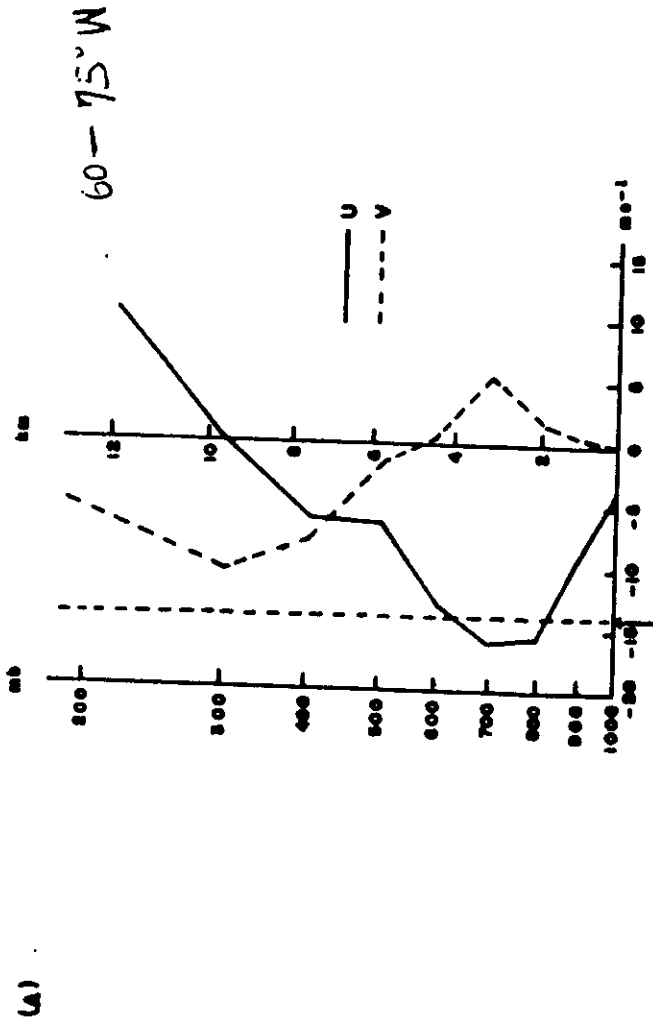


FIG. 14. WIND COMPONENT PROFILES FOR (A) VENEZUELA, (B) WEST AFRICA, AND (C) WEST PACIFIC REGIONS.

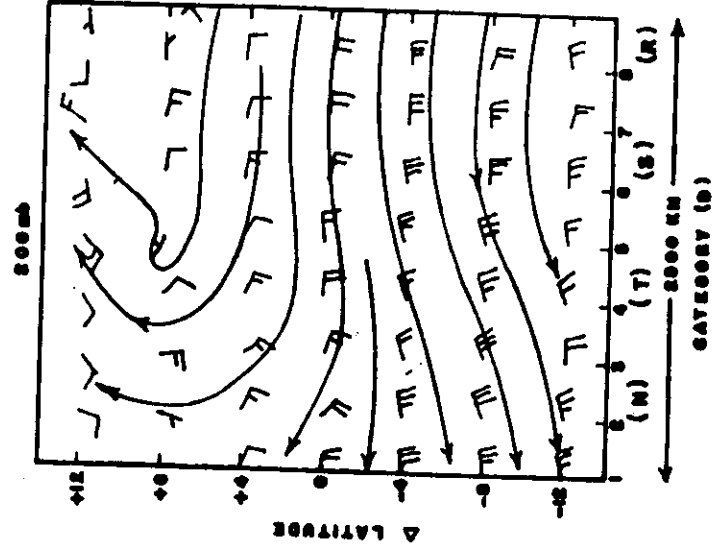
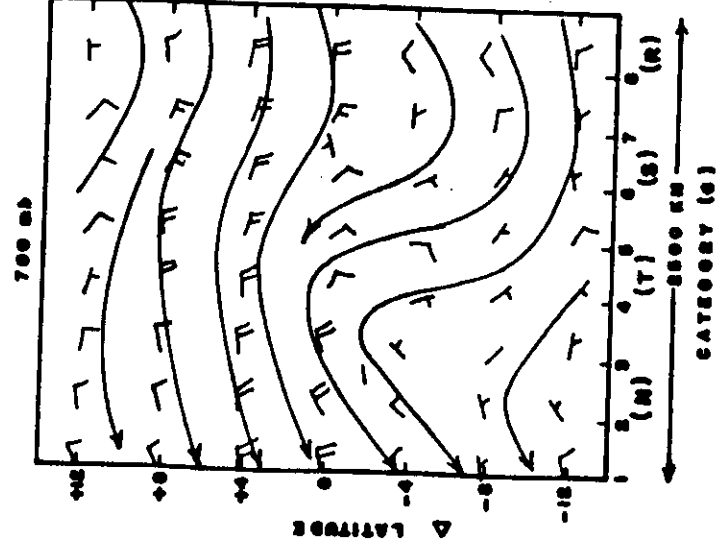
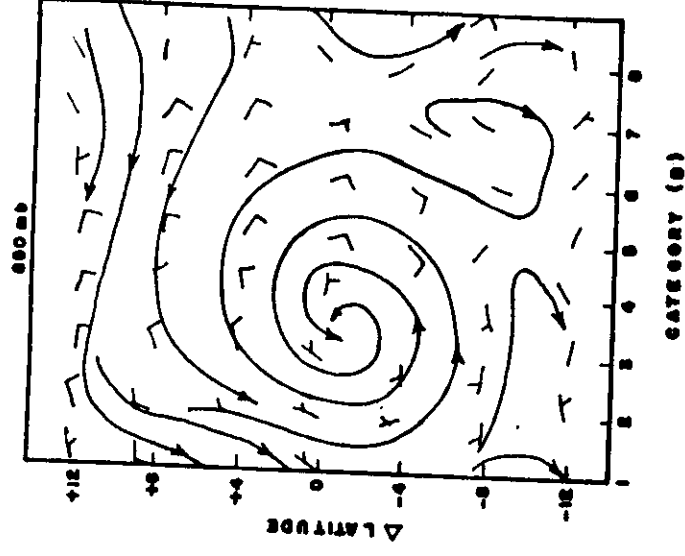
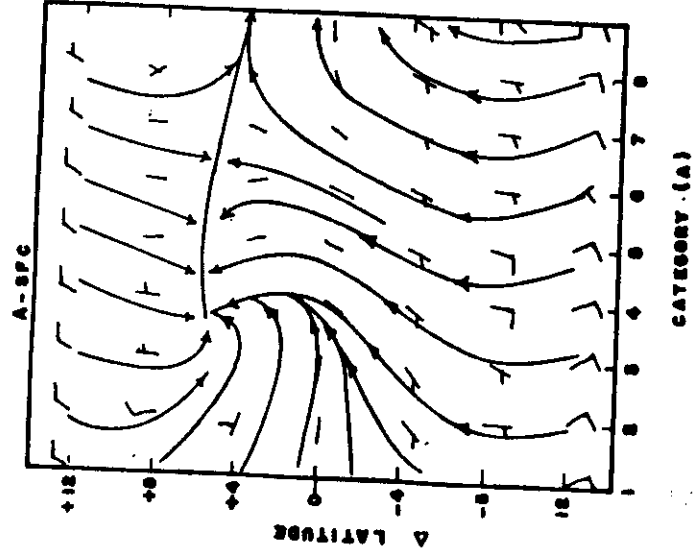


Fig.15- Streamline analyses of the total wind field associated with the waves at (A) surface, (B) 800mb, (C) 700mb, and (D) 200mb. The plotting convention has been designed so that one half barb equals 2.5 ms^{-1} and a full barb equals 5 ms^{-1} . The 0 latitude is approximately 11°N (taken from Reed et al, 1977)

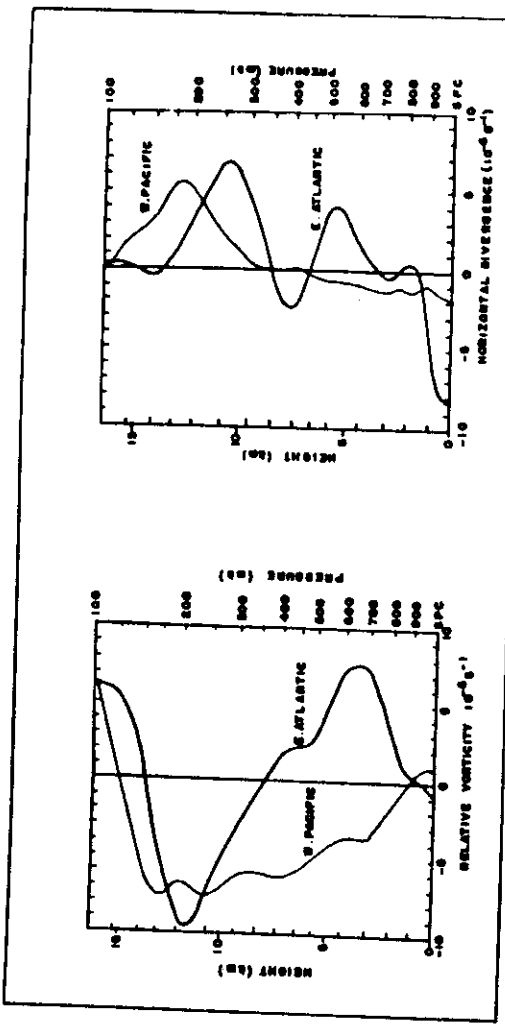


Fig. 16 Comparison of horizontal divergence and relative vorticity over Eastern Atlantic and West Pacific

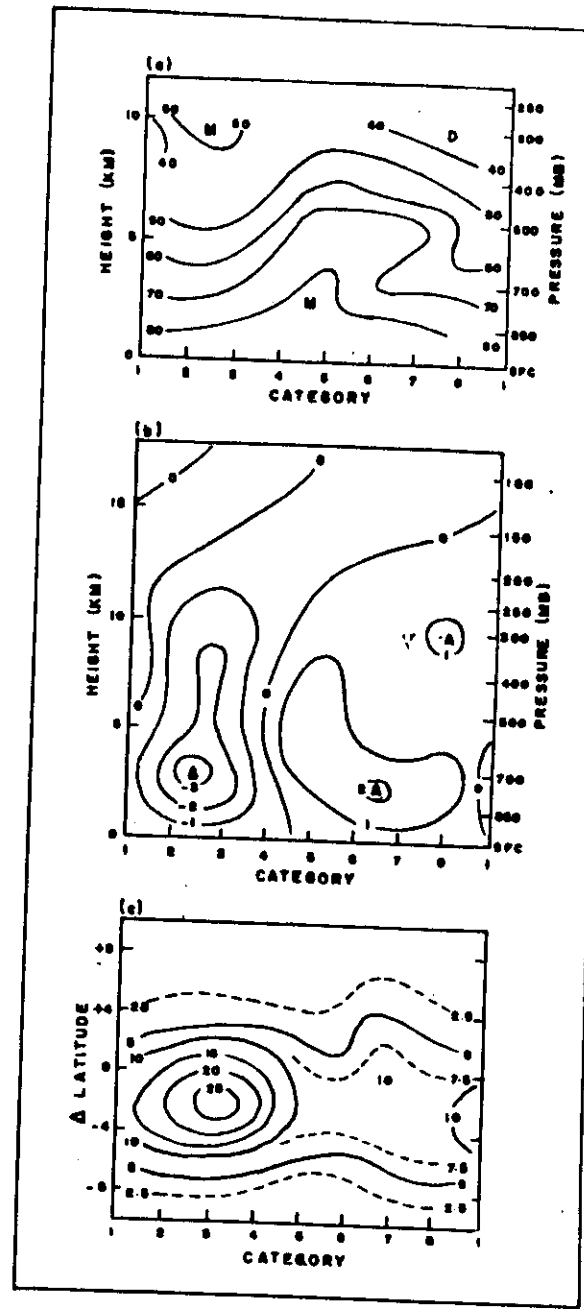
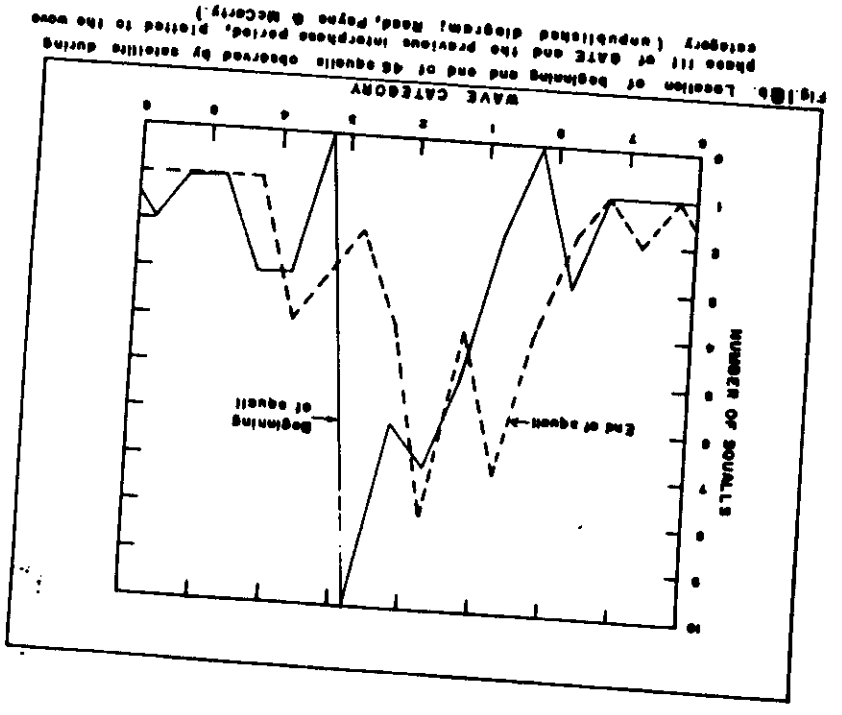
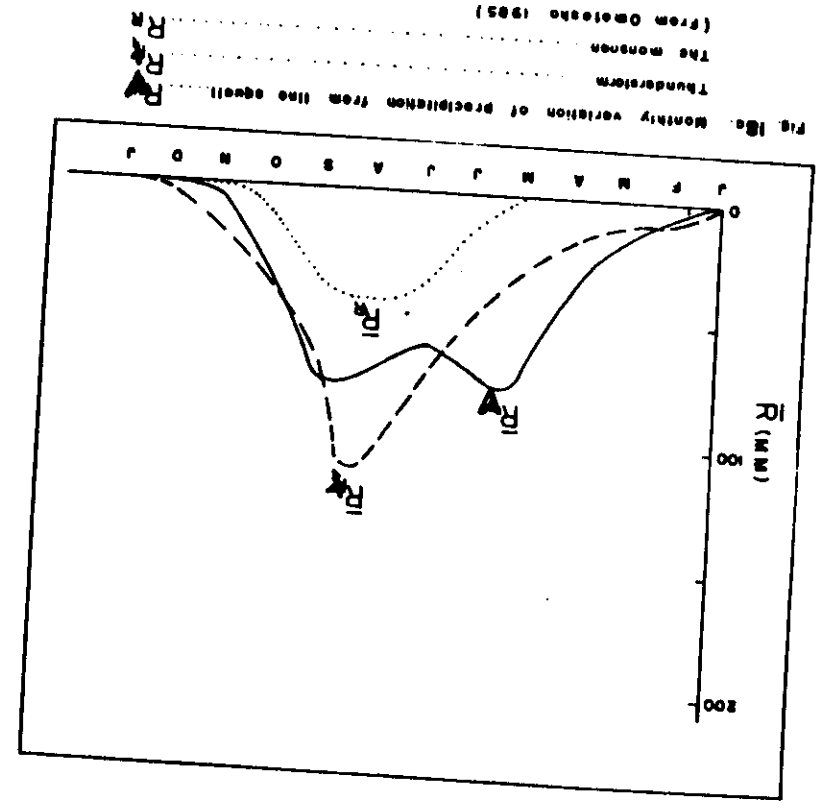


Fig. 17 (a) Vertical cross sections near 17°N of (a) Relative humidity in percent
(b) Vertical velocity in mb h⁻¹
(c) Map of rainfall amounts in mm day (reproduced from Reed et al. [10])



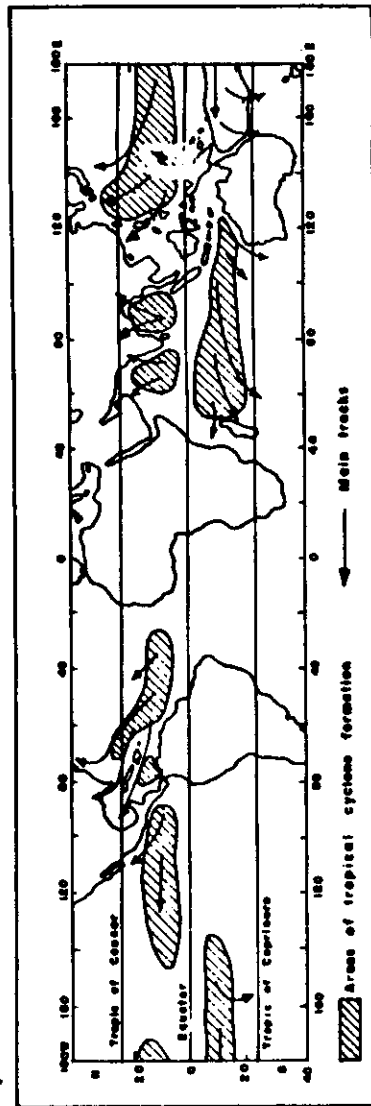


Fig 22a Formation and movements of tropical cyclones

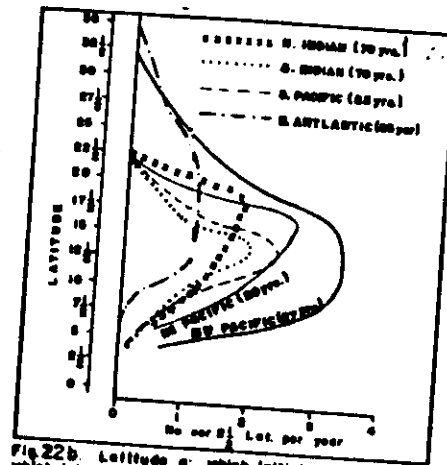


Fig 22b Latitude at which initial disturbances which later become tropical storms were first detected for the various development regions. Number of years in data coverage in parenthesis.

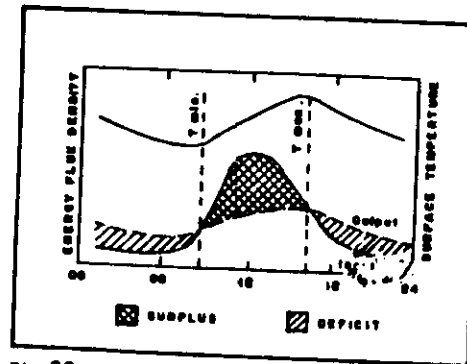


Fig 25 The relationship between surface energy exchange and the diurnal surface temperature regime.

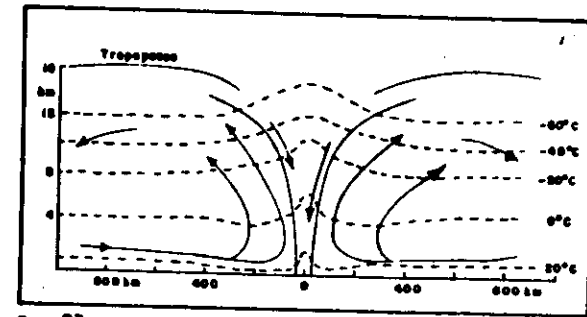


Fig 23 Cross-section of a tropical cyclone. Vertical elongation about 50 times.

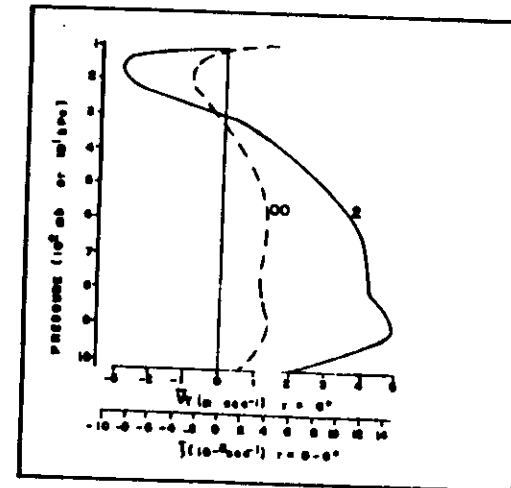


Fig 24 Mean relative vorticity within the area $r = 0-6^\circ$ (equivalent to mean tangential winds in $r = 6-7^\circ$ band) from Zehr's (1976) developing (stage 2) and non-developing (stage 0C) disturbances

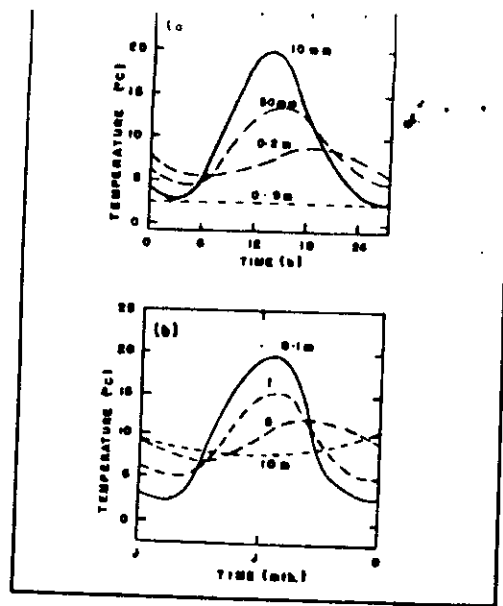


Fig 26 (a & b) Generalized cycles of soil temperature at different depths for (a) daily and (b) annual periods.

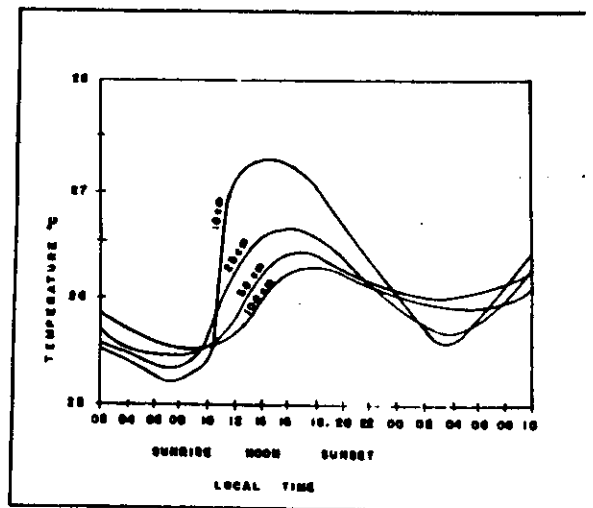


Fig 26c Temperature variation below the ground at Ile-Ife, Nigeria. (after Babalunde & Bologun, 1983).

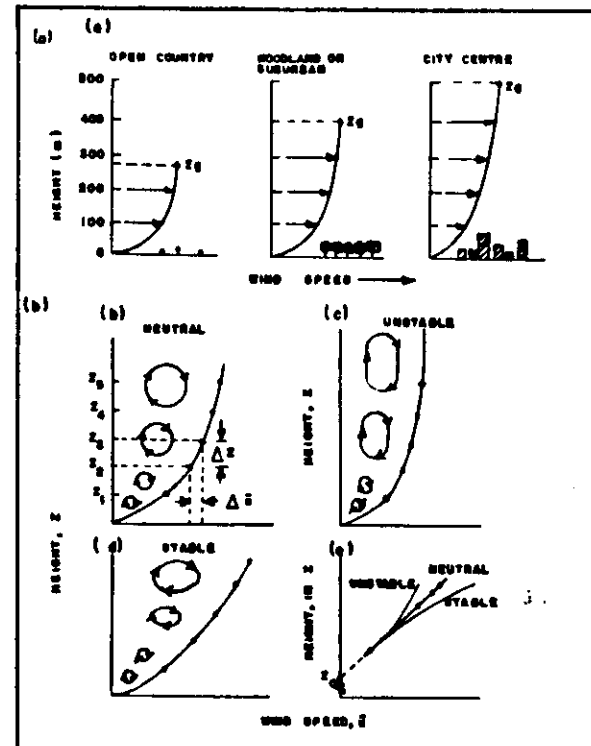


Fig 27. The wind speed profile near the ground showing the effect of stability on profile shape and eddy structure.

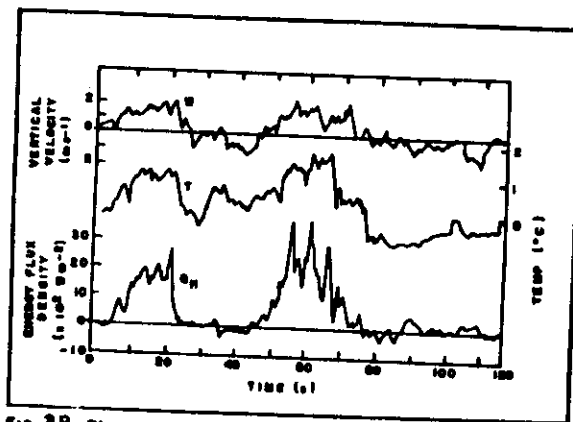


Fig. 28 The relationships between vertical velocity (w) and temperature (T) fluctuations, and the instantaneous sensible heat flux.

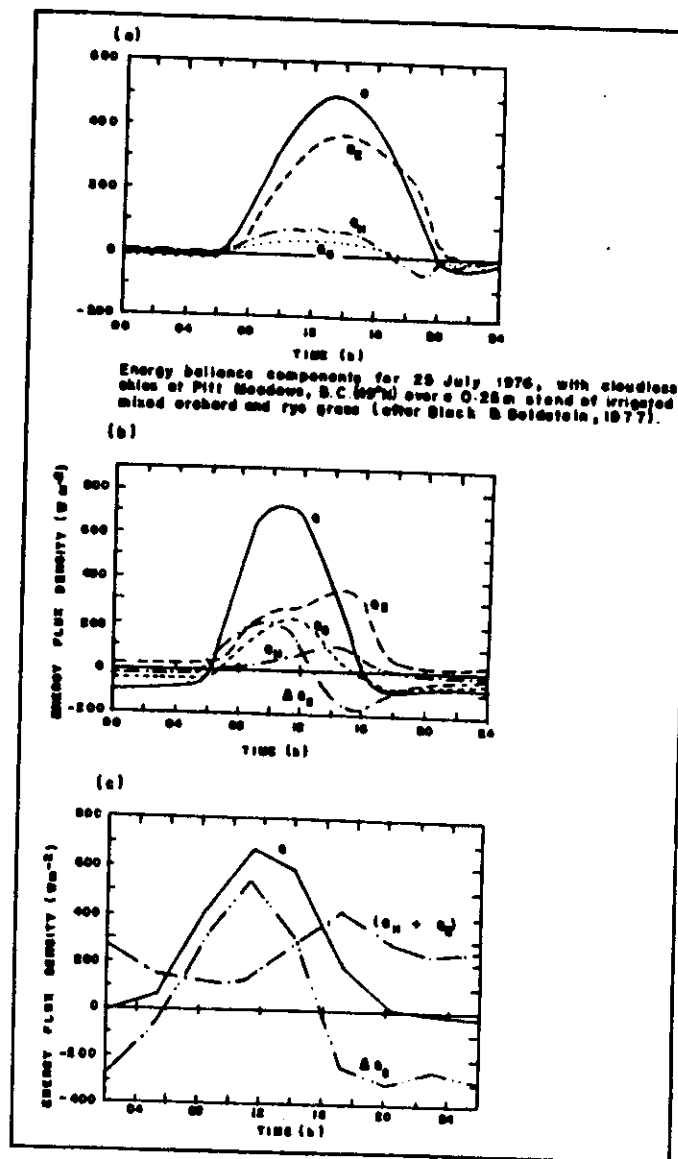


Fig. 29 (a, b & c) Diurnal variation of the energy balance components in and above (b) a shallow water layer on a clear September day in Japan (after Yabuki, 1957), and (c) the tropical Atlantic Ocean based on measurements from the ship Discoverer in the period 20 June to 2 July 1969 (after Holland 1971).